Regulation of xenobiotic efflux systems in Escherichia coli in response to environmental changes

著者	YAMAMOTO Kentaro
著者別名	山本 健太郎
その他のタイトル	環境変化に応じた大腸菌異物排出システムの制御
page range	1-89
year	2016-03-24
学位授与番号	32675甲第376号
学位授与年月日	2016-03-24
学位名	博士(生命科学)
学位授与機関	法政大学 (Hosei University)
URL	http://hdl.handle.net/10114/12385

法政大学審査学位論文

環境変化に応じた大腸菌異物排出システムの制御

法政大学大学院　理工学研究科　生命機能学専攻

山本健太郎

2016 年 3 月

Doctoral Dissertation

March, 2016

Regulation of xenobiotic efflux systems in *Escherichia coli* in response to environmental changes

Kentaro Yamamoto

Department of Frontier Bioscience,

Graduate School of Science and Engineering,

Hosei University

Table of contents

Abstract

The rising incidence of bacterial multidrug resistance has become a serious worldwide issue. The resistance-nodulation-cell division (RND)-type xenobiotic efflux system plays a major role in multidrug resistance of gram-negative bacteria. The only constitutively expressed RND system of *Escherichia coli* consists of the inner membrane transporter AcrB, the membrane fusion protein AcrA, and the outer membrane channel TolC. The latter two components are shared with another RND-type transporter AcrD, the expression of which is induced by environmental stimuli. In CHAPTER II of this study, I demonstrate how the RND-type ternary complexes, spanning the two membranes and the cell wall, are formed *in vivo*. Most foci of AcrB fused to green fluorescent protein (GFP) were fixed in the presence of TolC but showed lateral displacements when *tolC* was deleted. The fraction of fixed AcrB-GFP foci decreased with increasing levels of AcrD. I therefore propose that AcrD replaces AcrB in the complex with AcrA and TolC through a process I named "transporter exchange." Moreover, transporter exchange was suppressed by AcrB-specific substrates, suggesting that the ternary complex is stabilized when it is in action. These results suggest that the assembly of the RND-type efflux system is dynamically regulated in response to external stimuli, shedding new light on bacterial adaptive antibiotic resistance.

Indole plays important roles in a wide variety of bacterial physiology such as

virulence, drug resistance, persister cell formation, motility, and quorum sensing, among other diverse physiological processes. The expression of the inner membrane transporter gene *acrD* is induced by the presence of high concentrations of indole via a two-component system (TCS) consisting of the sensor kinase BaeS and the response regulator BaeR. In CHAPTER III of this study, I first observed GFP-fused AcrD encoded by the chromosomal gene with the native promoter. Observation of AcrD-GFP foci required very high concentrations of indole. In contrast, AcrD-GFP foci were readily detected in a *tolC*-deletion derivative strain without exposing to exogenous indole. The deletion of the tryptophanase gene *tnaA* or the TCS genes *baeSR* abolished the constitutive expression of AcrD-GFP in the *tolC*-deleted strain. I next measured indole concentrations in the presence and absence of TolC. The intracellular concentration of indole in the *tolC*-deleted strain was about three times as high as that in the parental strain. In contrast, TolC had little effect on the extracellular concentration of indole. These results suggest that TolC is involved in indole efflux. Moreover, I examined whether the interaction between TolC and an inner membrane transporter is required for indole efflux. A mutant TolC protein, defective in coupling to the inner membrane transporter, decreased the level of accumulation of intracellular indole, though not as effectively as the wild-type protein. It was suggested that TolC provides a channel not only for drugs but also for indole to diffuse out of cell, and that *E. coli* monitors changes in the intracellular concentration of indole rather than extracellular one.

Fluorescent proteins such as GFP have been used for labeling a cellular proteins. However, their large molecular weight of fluorescent proteins often interfere with the function of host protein, which would lead us to misdirected interpretations. In CHAPTER IV of this study, I applied florescent labeling methods other than fluorescent proteins to xenobiotic efflux and environment signaling systems. The fluorescein arsenical hairpin (FlAsH) specifically binds to a short peptide sequence of Cys-Cys-Pro-Gly-Cys-Cys (TC-tag), and it becomes fluorescent only when it binds covalently to a TC-tag. The TC-tagged outer membrane channel TolC of a part of the RND efflux system was labeled by FlAsH. This method resulted in the lateral localization of TolC without loss of their host functions. Moreover, I also used this FlAsH labeling method for the cytoplasmic signaling protein of *Vibrio cholerae*. I observed that the GFP-fused histidine kinase CheA1 of *V. cholerae* was localized to a cell pole and lateral region of the membrane with standing incubation or in the presence of sodium azide (NaN_3) that inhibits cytochrome *c* oxydase, whereas the protein was diffused in cellular cytosol without such treatments. The localization pattern of TC-tagged CheA1 was consistent with those of the GFP fusions, arguing strongly that the behaviors of CheA1-GFP reflects the localization of the native protein. Next, I visualized the taurine/amino acid chemoreceptor Mlp37 of *V. cholerae in vivo* by using the fluorescently labeled L-serine 5(6)-carboxyfluorescein ester (Ser-FAM). Upon treatment with Ser-FAM, fluorescent spots were detected at poles of cells expressing wild-type *mlp37*. Moreover, fluorescent spots of

Ser-FAM were decreased in the presence of non-fluorescent attractants serine and taurine, but not the weakest attractant L-glutamate, suggesting that the former attractants compete with Ser-FAM for binding to Mlp37. These results provide, for the first time, a tool to visualize direct ligand binding to a bacterial chemoreceptor *in vivo* and can also be applied to visualize signaling of TCSs and substrate transport in the xenobiotic efflux systems.

Acknowledgements

I would like to express my gratitude to Prof. Ikuro Kawagishi for a great deal of continuous advice, discussions and encouragements through the research.

I thank Drs. Akio Abe (Kitasato University), Tsutomu Sato (Hosei University), and Kaneyoshi Yamamoto (Hosei University) for giving invaluable advices as members of my doctoral dissertation committee.

I also thank Dr. Satoshi Murakami (Tokyo Institute of Technology) for invaluable discussion and encouragement, Dr. Yasushi Sako (RIKEN) for technical advices of image analysis, Dr. M. D. Manson (Texas A&M University) for critically reading the earlier version of the manuscript about the transporter exchange mechanism, Dr. Yoshiyuki Sowa (Hosei University) for all technical advices and allowing me to use the TIRFM system, and Dr. K. Yamamoto (Hosei University) for P1 phage strains and allowing me to use the spectrophotometer.

I would also like to thank Dr. Takehiko Inaba, Dr. So-ichiro Nishiyama, Dr. Yong-Suk Che, Dr. Satomi Banno, Dr. Hiroki Irieda, Dr. Hirotaka Tajima, Dr. Jun Teramoto, Dr. Yuki Yamanaka, Dr. Noriko Ohta, Ms. Tomomi Fujikawa and Ms. Natsumi Nonoyam for their supports and encouragements.

Strains from the Keio collection and plasmids from the ASKA clone were provided by the National BioResource Project - E. coli Strain at the National Institute of Genetics

(NBRP-E.coli at NIG). This work was supported by an MEXT KAKENHI Grant Number 24115519 and 24115518, the MEXT-Supported Program for the Strategic Research Foundation at Private Universities, 2008-2012 and Tokyo Institute of Technology Foundation Research and Educational Grants (26-reserch-013), 2013-2014.

List of abbreviations

- ABC ATP-binding cassette
- Ara arabinose
- CBPC carbenicillin
- CP chloramphenicol
- DMSO dimethyl sulfoxide
- EDT ethanedithiol
- EGFP enhanced green fluorescent protein
- FlAsH fluorescein arsenical hairpin binder
- GFP green fluorescent protein
- IMT inner membrane transporter
- IPTG isopropylthiogalactoside
- MATE multidrug and toxic compound extrusion
- MFP membrane fusion protein
- MFS major facilitator superfamily
- MIC minimum inhibitory concentration
- MINO minocycline
- MRSA methicillin-resistance *Staphylococcus aureus*
- MSD mean square displacement
- NA nalidixic acid
- NBRP national bioresource project
- NDM-1 New Delhi metallo-beta-lactamase-1
- OMC outer membrane channel
- PBP penicillin-binding protein

- PDDF pairwise difference distribution function
- PG peptidoglycan
- SMR small multidrug resistance
- TIRFM total internal reflection fluorescent microscope
- TM transmembrane
- TxRM Texas Red C_2 Maleimide
- RFP red fluorescent protein
- RND resistance-nodulation-division
- ROI region of interest
- Ser-FAM serine 5(6)-carboxyfluorescein ester
- sfGFP superfolder GFP
- TC-tag tetracysteine-tag
- TCEP tris-(2-carboxyethyl) phosphine
- TCS two-component regulatory system
- YFP yellow fluorescent protein

CHAPTER I

General Introduction

Bacterial antibiotic and multidrug resistance

Human has combated bacterial infections in this today. In 1928, Alexander Fleming incidentally discovered penicillin from a moldy petri dish and it had an ability to kill some bacteria. After 12 years, the other group at University of Oxford developed the mass-producing method of penicillin, and it was utilized as a therapeutic to treat patients of bacterial infection. For instance, in 1944, one of the deadly illnesses was tuberculosis which could be treated by streptomycin. Moreover, in 1950s, the various antibiotics including other than β-lactam as penicillin were discovered and used widely to pathogenic bacteria, which developed a chemotherapy (Davies & Davies, 2010).

However, in late-1950s, antibiotics leaded antibiotic resistant bacteria, which synthesis the enzyme as β-lactamase that inactivate antibiotics, to spread to a medical front. Now, it has been known over 900 β-lactamase are divided into 4 classes (A-D) based on amino acid sequence (Fig. I-1) (Davies & Davies, 2010; Matagne et al., 1999). These genes are coded on bacterial chromosomes or plasmids, and are transferred by transposons and mobile genetic elements such as R plasmids (Adams et al., 2008). Serine-β-lactamases as penicillinase are found in *Pseudomonas aeruginosa* and *Staphylococcus aureus*, and

Metallo-β-lactamases are found in *Escherichia coli, P. aeruginosa* (Bush et al., 1995; Garau et al., 2004; Lambert, 2002). These are hydrolytic enzymes to the ester and amide bond of β-lactam which causes inactivation of antibiotic activity. Especially, Metallo-β-lactamases lead gram-negative bacteria to achieve the resistance to new-generated antibiotic cephalosporin recently (Walsh et al., 2005). The β-lactams interfere with synthesis of peptidoglycan layer in cell wall. The peptidoglycan plays an important role in the rigid structure of cell wall which is essential to cell growth, division, and retaining cell form of bacteria. The penicillin-binding proteins (PBPs) are major enzymes involved in the synthesizing cross-linking of peptidoglycan layers (Spratt, 1977). The active sites of PBPs are targeted in an attack of β-lactam antibiotics and formed highly stable PBP-β-lactam complexes, which lead to inactivate the synthesis of bacterial cell walls (Nguyen-Disteche et al., 1982). The β-lactamases modify PBPs to reduce the affinity for β-lactams, which results in the resistance to β-lactam antibiotics (Dzidic et al., 2008).

The chloramphenicol and aminoglycosides interfere with protein synthesis by binding to each 50S and 30S ribosomal subunit of bacteria, respectively. An enzyme chloramphenicol transacetylase of gram-positive and -negative bacteria acetylates a hydroxyl group of chloramphenicol to prevent a binding of chloramphenicol to the 50S ribosomal subunit, which leads host strain to resist chloramphenicol (Morar & Wright, 2010). Also, the inactivating of aminoglycoside is caused by a phosphoryltransferase and adenylyltransferase

that modify the binding to the 30S ribosomal subunit, and its modification provides the resistance to aminoglycosides (Strateva & Yordanov, 2009).

In 1980, the active efflux system for tetracycline in *E. coli* was originally reported (McMurry et al., 1980), and now has been discovered in any bacteria. The xenobiotic efflux systems (pumps) transport antibiotics and toxic compounds for bacteria out of cell and keep the low levels of intracellular concentration of those (Nikaido, 1998; Webber & Piddock, 2003). Although some have drug-specificity, most of efflux systems are multidrug transporters that can transport various toxicants including drugs unrelated to structure and functional mechanism (Table. I-1). Thus, the multidrug efflux systems contribute pathogenic bacteria to resistance to a wide variety of antibiotics (Nikaido, 1998; Nikaido, 2000; Putman et al., 2000). The drug efflux transporters are classified into five categories: the major facilitator (MFS), small multidrug resistance (SMR), multidrug and toxic compound extrusion (MATE), ATP-binding cassette (ABC) and resistance-nodulation-cell division (RND) superfamilies (Li & Nikaido, 2009; Paulsen et al., 1996; Putman et al., 2000). A predominant cause of multidrug resistance of gram-negative bacteria is elevated expression of multidrug efflux transporters of the RND family (Nikaido, 1998). These systems comprise the inner membrane transporter (IMT), the outer membrane channel (OMC), and the membrane fusion protein (MFP) that is anchored to the inner membrane via a lipid moiety and bridges IMT and OMC (Nishino & Yamaguchi, 2001a; Paulsen et al., 1996). This transporter superfamily is

ubiquitous in nature, including higher animals and plants (Altmann et al., 2004).

Use of many antibiotics over the years, the increasing use of antibiotics leading to the emergence of multidrug resistant bacteria is responsible for serious social problems. Our pace of the discovering new antibiotics has been slowed exponentially while the appearance of novel variants of multidrug resistant bacteria has increased. The methicillin was developed as a first designed β-lactam antibiotic to resist to a penicillinase-producing pathogenic bacteria such as *S. aureus*. After 3 years, however, the methicillin-resistance *S. aureus* (MRSA) which has resistance to many β-lactam antibiotics emerged and caused a serious bloodstream infection in the clinical front. Recently, it had enormous impacts on society that the spread of super multidrug resistant bacteria across the entire world was reported. This bacteria have the resistance to almost all β-lactam antibiotics, fluoroquinolone and aminoglycoside by New Delhi metallo-beta-lactamase (NDM-1) (Gelband & Laxminarayan, 2015). The potent drug resistant bacteria have threatened our public health, and also multidrug resistant bacteria have killed over 700,000 patients every year in the world (Shallcross et al., 2015). We have no perfect antibiotic that is effective in every bacteria without adverse effects, and also we are required a non-traditional proactive approach to multidrug resistant bacteria.

Indole

Indole occurs widely throughout nature environment. Over the past 100 years,

bacteria produces indole have been found and used for bacterial taxonomy, identification and diagnostic test (Smith, 1897). Now at least 85 bacterial species including pathogenic Gram-negative and positive bacteria are known to produce a quantity of indole (Lee & Lee, 2010). Indole is synthesized from amino acid tryptophan by tryptophanase, which is a cytoplasmic hydrolysis enzyme to reduce tryptophan to indole, pyruvate and ammonia. In *Escherichia coli*, these reactions are catalyzed by the tryptophanase TnaA (Stewart & Yanofsky, 1985) and many other proteins; tryptophan specific transporter TnaB, AroP, tryptophanase leader peptide TnaC, trp operon leader peptide TrpL and so on (Li & Young, 2013). The indole biosynthesis is down regulated by environmental factors, such as a high concentration of glucose as carbon source (Wyeth, 1919), a high temperature (indole synthesis is stopped at 44.5°C) (Bueschkens & Stiles, 1984; Li et al., 2003), a low pH (TnaA is most induced at pH9.0) (Blankenhorn et al., 1999; Wyeth, 1919), and a cell density (Kobayashi et al., 2006). Biosynthetic indole has long been known to work as a chemorepellent of *E. coli* (Tso & Adler, 1974), and recently has also been learned as a chemical signaling molecule to an intra- and interspecies of bacteria which involve in the expression of many genes (Melander et al., 2014). The signaling of indole regulates the bacterial virulence (Hirakawa et al., 2009), drug resistance (Hirakawa et al., 2005), biofilm formation (Di Martino et al., 2002), genetic stability (Chant & Summers, 2007), persister cell formation (Vega et al., 2012), motility (Lee et al., 2007), and quorum sensing (Lee & Lee, 2010), among other diverse

physiological processes. It also has been known that indole is stable in *E. coli* cell because of no pathway of indole degradation and modification by enzymes (Chant & Summers, 2007; Lee & Lee, 2010). Moreover, the equilibrium of indole and its metabolism involve in an intestinal tract inflammation of mammalian (Bansal et al., 2010). Indole and derivations of tryptophan-metabolite play an important role in the regulation of broad-ranging physiology in bacteria and animals (Fig. I-2).

Fluorescein arsenical hairpin binder (FlAsH) labeling

Fluorescence microscopy has been used for the study of protein localization and dynamics with a variety of chemical labeling methods. The discovery of green fluorescence protein (GFP) from the jellyfish *Aequorea victoria* (Shimomura et al., 1962) enable a fluorescent live-cell imaging using GFP fused host protein chimera. Moreover, GFP variants have been developed, such as enhanced GFP (EGFP) (McRae et al., 2005), superfolder GFP (sfGFP) (Pedelacq et al., 2006), and yellow fluorescence protein (YFP) (Ormo et al., 1996), and were utilized in various situations in cell biology. In spite of these benefits, fluorescence proteins were limited on use due to their large molecular weight. This molecular size interferes with the function, stability, and localization of their fused host protein (Swulius & Jensen, 2012). The fluorescein arsenical hairpin binder–ethanedithiol (FlAsH-EDT_2) has been developed as an alternative approach for specific labeling in live-cell imaging (Griffin et al.,

1998). FlAsH specifically binds to a short peptide sequence of Cys-Cys-Pro-Gly-Cys-Cys (TC-tag), and it forms intermolecular disulfide linker. FlAsH is complexed with EDT as a weakly fluorescence, and it becomes a fluorescence with binding to a TC-tag whose excitation and emission peaks are 508 and 528 nm, respectively. The equilibrium of FlAsH-EDT_2 and FlAsH-TC depend on the concentration of EDT. In HeLa cell, FlAsH-TC is likely to be stable at $\leq$ 10 μM EDT which returned to a FlAsH-EDT_2 as non-fluorescence state at $\geq$ 1 mM EDT (Griffin et al., 1998). FlAsH labeling technique is useful for live-cell imaging as an alternative to fluorescence proteins.

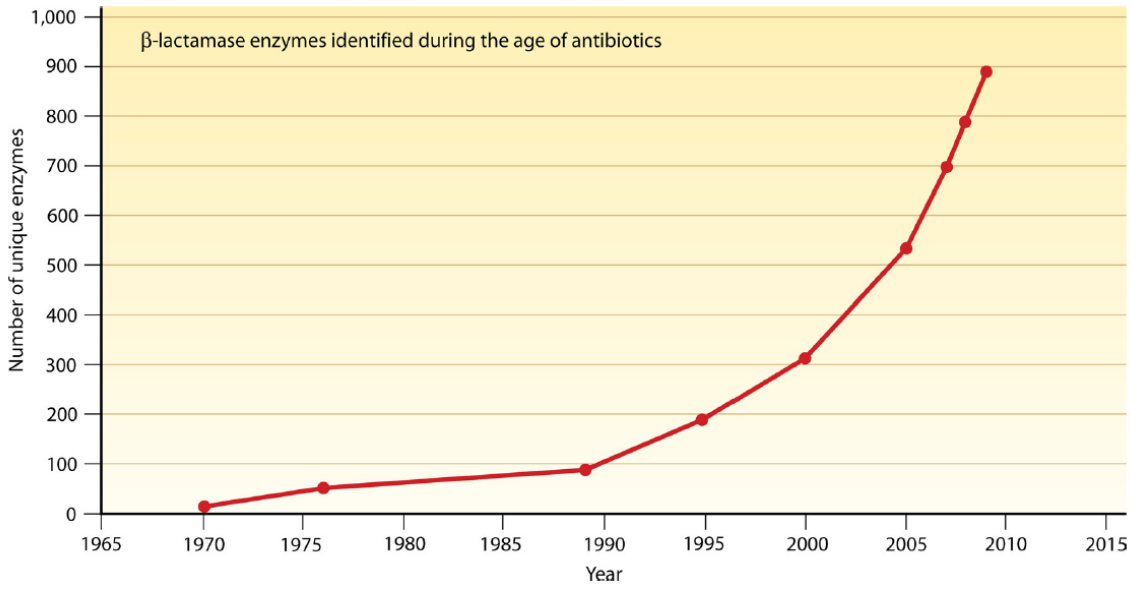

Fig. I-1. Increasing of number of identified β-lactamase.

Number of β-lactamase, which inactivates β-lactam class of antibiotics, is on the increase. (cited from Davies & Davies, 2010)

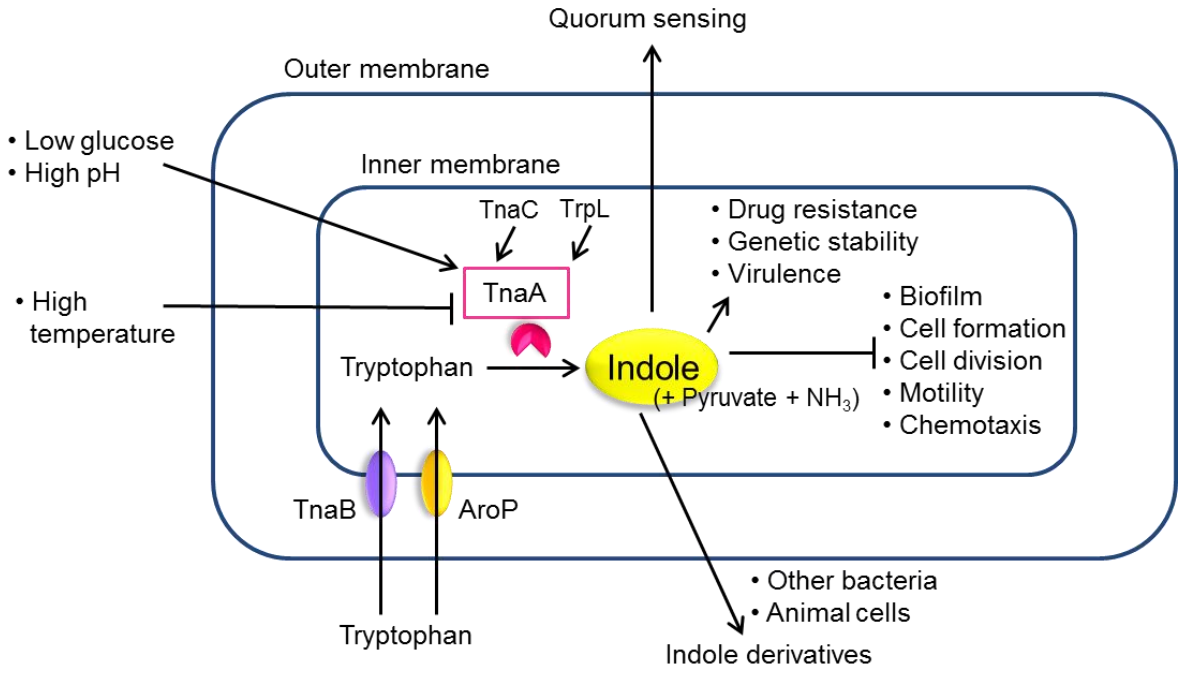

Fig. I-2. Indole biosynthesis and signaling pathway in *E. coli*.

This figure shows that the regulations of indole biosynthesis and indole-induced phenotype. Arrows and bar-head lines indicate up and down-regulation of gene expression or phenotype, respectively.

Bacterial species	Efflux system	Antibitic resistance of interest
E. coli	AcrAB-TolC	β-lactams, chloramphenicol, tetracycline, minocycline, fluoroquinolones, nalidixic acid, deoxycholate, SDS
	AcrAD-TolC	tetracycline, kanamycin, deoxycholate, carbenicillin
	MdtABC-TolC	novobiocin, nalidixic acid, deoxycholate
	EmrE	acriflavine, benzalkonium
S. aureus	MepA	tetracycline, minocycline, ciprofloxacin, norfloxacin
P. aeruginosa	MexAB-OprM	β-lactams, tetracycline, fluoroquinolones
	MexMY-OprM	aminoglycosides, chloramphenicol
A. baumannii	AdeABC	chloramphenicol, tetracycline, fluoroquinolones, aminoglycoside, erythromycin, trimethoprim

Table. I-1. Bacterial multidrug efflux systems and its substrates.

This table shows that the typical multidrug efflux systems of clinical pathogenic bacteria and the toxic compounds are transported by those systems.

CHAPTER II

Substrate-dependent dynamics of the multidrug efflux transporter AcrB of *Escherichia coli*

Introduction

The increasing use of antibiotics has led to the emergence of multidrug resistant bacteria, a phenomenon that has serious consequences for public problems. A predominant cause of multidrug resistance of gram-negative bacteria is elevated expression of multidrug efflux transporters of the RND family (Nikaido, 1998) (Fig. II-1). These systems comprise an inner membrane transporter (IMT), an outer membrane channel (OMC), and a membrane fusion protein (MFP) that is anchored to the inner membrane via a lipid moiety and bridges IMT and OMC (Nishino & Yamaguchi, 2001a; Paulsen et al., 1996). This transporter superfamily is ubiquitous in nature and is found in prokaryotes and eukaryotes, including higher animals and plants (Altmann et al., 2004). The RND efflux systems of *Escherichia coli* and *Pseudomonas aeruginosa* have been extensively studied in terms of their biochemistry, molecular architecture, and patterns of gene expression (Stover et al., 2000). Among the five RND transporters of *E. coli*, only the AcrB-AcrA-TolC complex (hereafter referred to as AcrBA-TolC) is constitutively expressed (Sulavik et al., 2001) and plays a major role in its multidrug resistance (Nikaido, 1998; Okusu et al., 1996; Zgurskaya & Nikaido, 1999). The

structure-function relationship of the IMT AcrB is well studied. The proton-drug antiporter AcrB (Paulsen et al., 1996), which forms a homotrimer of 12-transmembrane (TM) subunits (Murakami et al., 2002), captures a wide variety of antibacterial compounds, including antibiotics, detergents and other amphiphilic agents, and directly transports these substrates out of the cell via TolC (Nikaido, 2000; Zgurskaya & Nikaido, 1999). TolC is also a homotrimeric protein consisting of an outer membrane domain folded into a 12-stranded β-barrel. It has a periplasmic extension (about 100 Å in length) with an α-helical coiled coil domain and a mixed α/β equatorial domain, which together form a hollow cylindrical structure that allows substrate to diffuse directly out of the cell (Koronakis et al., 2000). Whereas the TolC homotrimer has three-fold symmetry (Koronakis et al., 2000), the AcrB homotrimer is asymmetric, and each protomer plays a different role in substrate binding (Murakami et al., 2006). The functional association of AcrB with TolC is thought to require the MFP AcrA (Ma et al., 1993), the stoichiometry of which has not been unambiguously determined. However, a recent cryo-EM study suggests that AcrA forms a homohexamer (Du et al., 2014).

The transcription of various inducible xenobiotic efflux genes is regulated by two-component regulatory systems (TCSs) (Nishino & Yamaguchi, 2001b; Nishino & Yamaguchi, 2002), each typically consisting of a sensor kinase and a response regulator, which are widely distributed among prokaryotes and eukaryotes. The *E. coli* genome encodes

62 TCS proteins that mediate a variety of environmental responses (Kofoid & Parkinson, 1988; West & Stock, 2001). Most RND genes encoding MFP/IMT pairs, including *acrA/acrB*, are located in tandem on the chromosome and form transcriptional units (Fig. II-2). Among all IMT genes, only the *acrD* gene stands alone. Its product, AcrD, is closely related to AcrB and also interacts with AcrA and TolC (Aires & Nikaido, 2005), the latter of which is encoded by a gene belonging to a separate operon (Fig. II-2). The AcrDA-TolC complex exports aminoglycosides and anionic β-lactams, such as carbenicillin and sulbenicillin, which are not transported by AcrB (Kobayashi et al., 2014; Nishino et al., 2003; Rosenberg et al., 2000). The expression of *acrD* is induced upon the addition of indole to culture media via the TCS consisting of the sensor kinase BaeS and the response regulator BaeR (Hirakawa et al., 2005; Nishino et al., 2005).

These properties raise an important question concerning assembly of the ternary complex. Do newly synthesized AcrD molecules assemble into a ternary AcrDA-TolC complex *de novo*, or do they replace AcrB subunits in the pre-existing AcrBA-TolC complex? It may be advantageous for bacteria to employ the latter mechanism, which we call "transporter exchange," to remove harmful substrates promptly out of cells as quickly as possible. However, it has not been established how RND-type transporter complexes that bridge two separate membranes are assembled. These considerations, and the pioneering study on single molecule behaviors of bacterial membrane proteins (Leake et al., 2006), led us

to study the assembly and dynamics of the AcrB/D AcrA TolC protein complex *in vivo*.

I visualized AcrB *in vivo* using green fluorescent protein (GFP). Observations with total internal reflection fluorescence (TIRF) microscopy revealed that most fluorescent foci of AcrB-GFP were stationary and mobile in the presence and absence of TolC, respectively. I next examined the effect of AcrD on the dynamics of AcrB. The fraction of mobile AcrB-GFP foci increased with increasing levels of AcrD. I therefore propose that the AcrBA-TolC complex becomes unstable upon the induction of AcrD, which presumably replaces AcrB in the ternary complex. Moreover, such instability is suppressed upon the addition of AcrB-specific substrates. These results suggest that the assembly of the RND-type efflux system is a regulated dynamic process that provides bacteria with a highly flexible repertoire of survival strategies to cope with a wide spectrum of antibiotics.

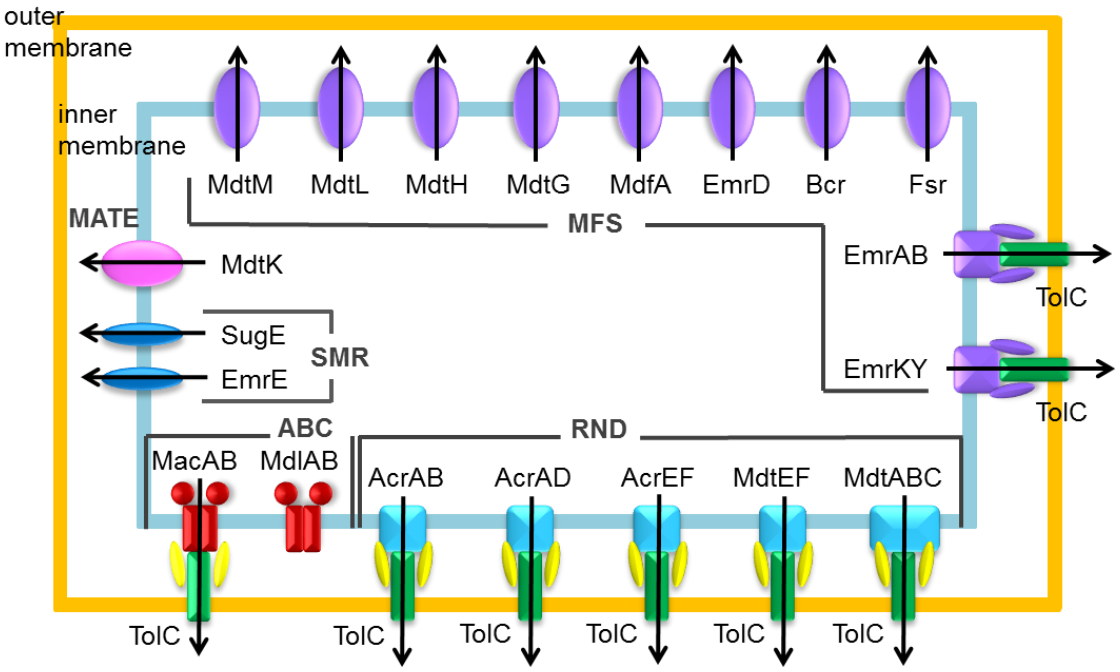

Fig. II-1. Xenobiotic efflux protein families in *E. coli*.

RND-type: Forms a tripartite complex. Captures a wide variety of toxic compounds and directly transports them out of cell via the outer membrane channel TolC. Plays a major role in multidrug resistance of gram-negative bacteria. MFS-type: The major membrane transporter family. A drug/proton antiporter with 12-14 transmembrane domains. Plays a major role in xenobiotic efflux by gram-positive bacteria. SMR-type: Related to the MFS-type but has 4 transmembrane domains. MATE-type: Related to the MFS-type but is driven by sodium ion. ABC-type: The ATP-binding-cassette-type with 4 transmembrane domains.

Results

The AcrB-GFP trimer is stationary in the cytoplasmic membrane via its association with TolC in the outer membrane.

I constructed a strain expressing green fluorescent protein (GFP)-fused AcrB from the chromosomal *acrB* locus (strain YKN12, a derivative of strain BW25113) (Datsenko & Wanner, 2000). The AcrB-GFP protein retained almost full activity as judged by the minimal inhibitory concentrations (MIC) of AcrB substrates (Fig. II-3B). To assess the effect of TolC on the AcrB-GFP dynamics within the cell membrane, I constructed a *tolC*-deleted derivative of YKN12 (strain YKN17). Immunoblotting with monoclonal anti-GFP antibody detected a band of AcrB-GFP without visible degradation products (Fig. II-4). The expression levels of the AcrB-GFP in a *tolC*-deleted strain was almost the same as that of the *tolC*$^{+}$ strain (Fig. II-4). TIRF microscopic observations detected a clear difference in the lateral displacements of AcrB-GFP foci between strains YKN12 (*tolC*$^{+}$) and YKN17 (Δ*tolC*) (Fig. II-5A, B, D). Fig. II-5A and D show the x-y trajectories and the time lapse images of AcrB-GFP foci in these genetic backgrounds. AcrB-GFP movement (an AcrB subunit with 12 TMs has a molecular mass of 110 kDa) was analyzed by monitoring two-dimensional mean square displacements (MSD) of individual foci over time. In the presence of TolC, the calculated MSD values of all AcrB-GFP foci tested at time 330 ms were distributed below 0.5×10^{-2} μm^2, with an average of 0.2 ± 0.1 (mean ± S.D.) $\times 10^{-2}$ μm^2 (Fig. II-5B, 6A). In the absence of TolC, most

AcrB-GFP foci moved incessantly, and their MSD values were distributed over a wide range: 2.3−10.7 × 10^{-2} μm^2, with an average of 5.2 ± 2.2 (mean ± S.D.) × 10^{-2} μm^2 (Fig. II-5B, 6A). I then fitted the data (*i.e.* the averaged MSD-Δ*t* plots for stationary and mobile fractions of AcrB-GFP in strains YKN12 and YKN17) to linear regression models (Fig. II-6B). The diffusion coefficient (= *D*) values in the presence and the absence of TolC calculated from these fits are 6.8 ± 5.0 (mean ± S.D.) × 10^{-4} μm^2 s^{-1} and 3.5 ± 1.8 × 10^{-2} μm^2 s^{-1}, respectively. When complemented with a plasmid encoding TolC, MSD values of AcrB-GFP foci and resistance to nalidixic acid returned to levels comparable to those of the parent strain (Fig. II-3B, 5B). AcrB-GFP foci in the *tolC*$^+$ and the complemented strains showed about two orders of magnitude smaller *D* values (8.0 ± 4.0 × 10^{-4} μm^2 s^{-1}) than those in the Δ*tolC* strain. The former can be regarded as immobile within experimental errors. Based on these data, foci with MSDs at time 330 ms below and above 0.5 × 10^{-2} μm^2 (marked with a dotted line in Fig. II-5B) will hereafter be designated as “stationary” and “mobile,” respectively. Accordingly, all the AcrB-GFP foci in the *tolC*$^+$ background are stationary and those in the Δ*tolC* background are mobile, whereas 84% of those in the complemented strain are stationary (Fig. II-5C). In the *tolC*$^+$ background, time-course analyses of the fluorescence emission from single stationary AcrB-GFP foci detected up to three-step photobleaching (Fig. II-7A). Fig. II-6B shows the power spectrum of one focus as the pairwise differences (Pairwise Difference Distribution Function, PDDF), which indicated the step size of single molecular GFP, with an

average of 680 ± 180 (mean ± S.D., arbitrary unit) under my experimental conditions (Fig. II-7B, C). The distribution of intensity at the first frame peaked at a value that is about three times the intensity of a single GFP estimated by photobleaching (Fig. II-7D).

Visualization of TolC with a fluorescent reagent.

I next examined whether stationary AcrB-GFP foci in the inner membrane indeed co-localize with TolC in the outer membrane. Substituting Cys for Ala-269 in an extracellular loop of TolC (11 residues in length; Fig. II-8A) did not affect the drug efflux activity as judged from MIC of nalidixic acid (Fig. II-3B). TolC-A269C was stained with the thiol-reactive fluorescent reagent Texas Red maleimide (TxRM) at low concentrations for a short period of time to minimize non-specific labeling of other Cys-containing proteins. TIRF microscopy detected foci of labeled TolC-A269C, some of which co-localized with AcrB-GFP (Fig. II-8B). No foci were observed in cells expressing wild-type TolC, demonstrating that non-specific labeling was negligible (Fig. II-8B).

AcrB dissociates from the preformed complex with TolC and AcrA upon induction of AcrD.

I was interested in determining whether the expression of AcrD, the closest homolog of AcrB, influences AcrB dynamics in the *tolC*$^{+}$ strain. First, AcrD was expressed from an

arabinose-inducible plasmid. The fraction of mobile AcrB-GFP foci increased (from 8% to 72%) with increasing concentrations (0−100 μM) of arabinose (Fig. II-9A, B) and increased (from 12% to 64%) over time (0−2 h) after the addition of 100 μM arabinose (Fig. II-9C, D). I suggest that the induction of AcrD facilitates dissociation of AcrB from the preformed complex with TolC and AcrA, presumably to from a new ternary complex (AcrDA-TolC). I then tested whether the dynamics of AcrB-GFP is influenced by the expression of AcrD from the native chromosomal gene. The expression of *acrD* was induced by the addition of indole or by overexpressing the TCS response regulator BaeR (Hirakawa et al., 2005; Nishino et al., 2005). I next constructed a strain (named MBRT02) carrying a chromosomal gene encoding AcrD-GFP (the design is essentially the same as *acrB-gfp* in strain YKN12). In strain MBRT02, AcrD-GFP foci were observed when cells were exposed to indole or when BaeR was overexpressed from the plasmid (Fig. II-10A). The increased expression of AcrD-GFP induced by plasmid pBaeR was verified by immunoblotting with monoclonal anti-GFP antibody (Fig. II-10B). Consistent with that result, the fraction of mobile AcrB-GFP foci in YKN12 cells treated with indole (60%) was larger than that in cells not exposed to indole (4%) (Fig. II-11A, B). Taken together, these results demonstrate that transporter exchange occurs in the native setting.

The AcrBA-TolC complex is stabilized by AcrB-specific substrates.

The findings just described raise the question of whether the induction of AcrD destabilizes the AcrBA-TolC complex while the latter complex is in the process of exporting its substrates. AcrBA-TolC, but not AcrDA-TolC, exports chloramphenicol and minocycline. When either of these substrates was added to the culture medium, the fraction of stationary AcrB-GFP foci became relatively insensitive to the expression of AcrD (32% without a substrate *vs* 84% with 4.9 μM chloramphenicol and 60% with 3.2 μM minocycline; Fig. II-11C, D). This was further examined under more physiological conditions: indole-induced expression of AcrD-GFP in MBRT02 cells. The functionality of the AcrD-GFP protein in these experiments was verified by checking MIC for an AcrD-specific substrate, carbenicillin (Fig. II-10C). The AcrB-specific substrate chloramphenicol decreased the fraction of stationary AcrD-GFP foci. I also examined whether the incorporation of IMT molecules into the ternary complex is affected by its substrate. The addition of the AcrD-specific substrate carbenicillin to cells expressing AcrD from the plasmid did not reduce the fraction of stationary AcrB-GFP (32% without a substrate *vs* 36% with carbenicillin; Fig. II-12). These results suggest that the AcrD-induced instability of the preformed AcrB-containing complex is suppressed when the preexisting complexes are transporting substrates, whereas the presence of a substrate of a second, newly synthesized transporter does not necessarily facilitate transporter exchange.

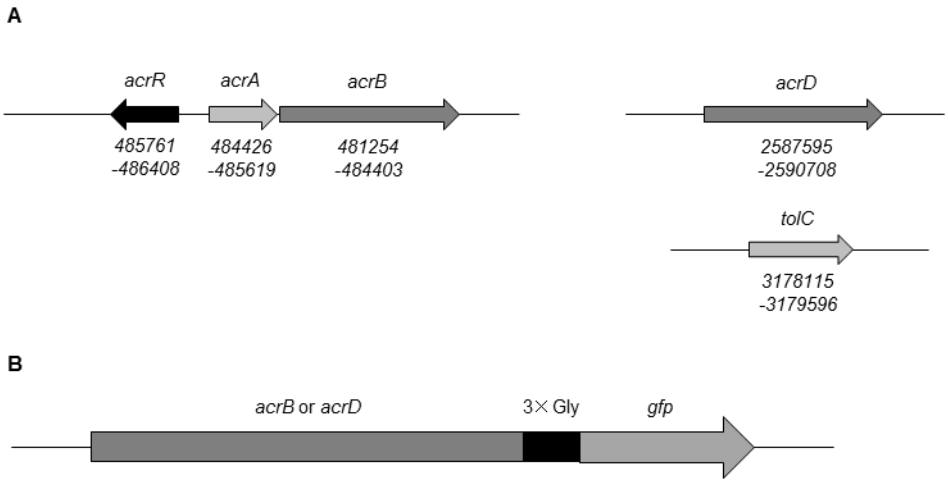

Fig. II-2. Characterization of AcrB-GFP and AcrD-GFP.

(A) The loci of RND-component genes on the chromosome of *E. coli* str. K-12 substr. MG1655. (B) Construction of AcrB-GFP and AcrD-GFP. GFP was fused to the carboxy-terminus of AcrB or AcrD through a Gly_3 linker.

A

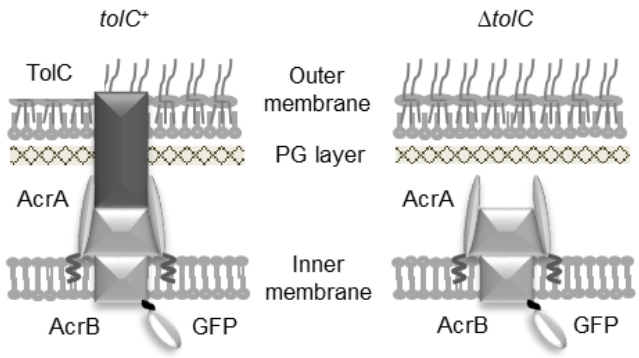

B

Drug	MIC (μg ml^{-1})						
	AcrB	AcrB-GFP	Δ*acrB*	Δ*tolC*	YKN17 (Δ*tolC*) harboring a plasmid encoding TolC		
					WT	A269C	none
CP	**3.13**	**3.13**	0.78	0.78	ND	ND	ND
NA	**3.13**	**3.13**	0.78	0.78	**1.57**	**1.57**	0.78

Fig. II-3. Design and MIC test of AcrB-GFP.

(A) Schematic illustration of AcrB-GFP in the cell surface of *E. coli*. For simplicity, AcrB is depicted to bind AcrA even in the absence of TolC, though it has not been experimentally tested. (B) Antibiotic susceptibility analysis. Wild-type AcrB and AcrB-GFP were expressed from the chromosomal genes of strains BW25113 and YKN12, respectively, while plasmid-encoded wild-type TolC (pKRB2100) and mutant TolC (A269C; pKRB2104) were expressed in strain YKN17 (Δ*tolC*). Bold face represents the resistance indicative of the significant efflux activity. Abbreviations: CP, chloramphenicol; NA, nalidixic acid; ND, not determined (due to the plasmid-borne CP resistance).

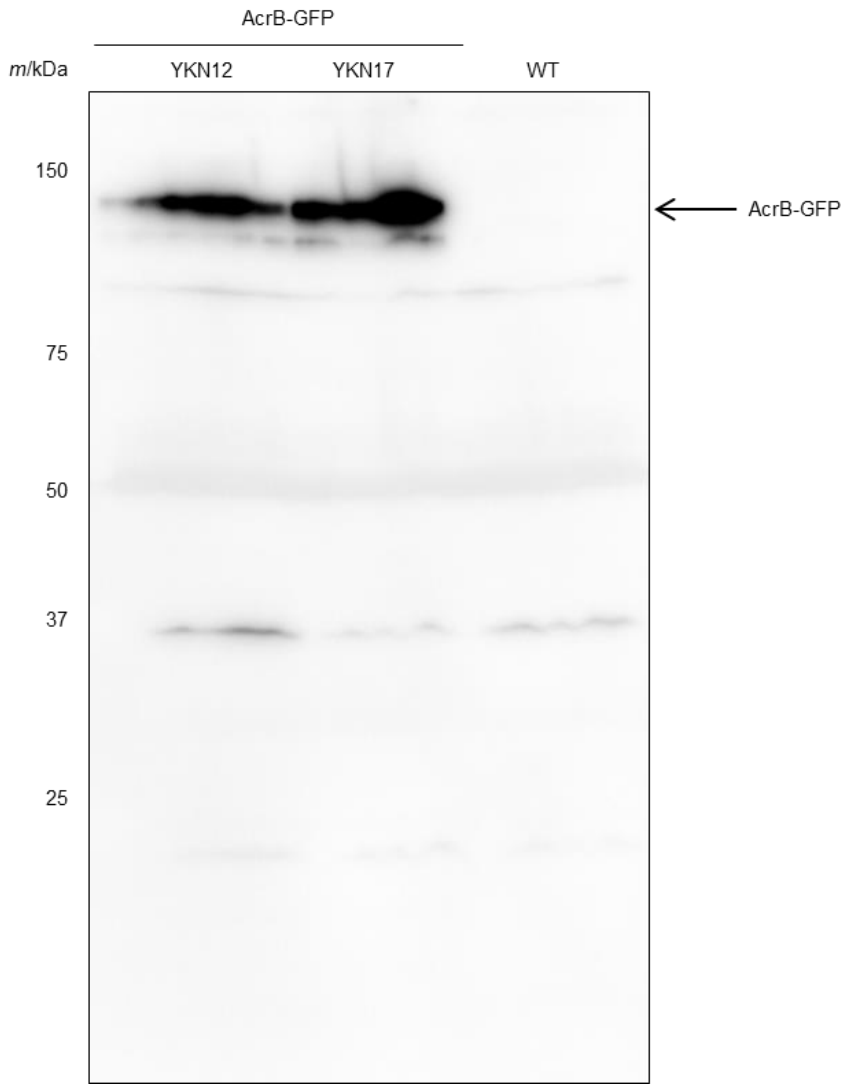

Fig. II-4. Detection of AcrB-GFP using immunoblotting.

AcrB-GFP (*m*/kDa = 140) was expressed in strains YKN12 (*tolC*$^{+}$) (left lane) and YKN17 (Δ*tolC*) (middle lane). The wild-type strain BW25113 was used as a control (right lane). Whole cell lysates were subjected to Western blotting with monoclonal antibody raised against GFP and anti-mouse-IgG (Cell Signaling Technology) antibody labeled with horse-radish peroxidase.

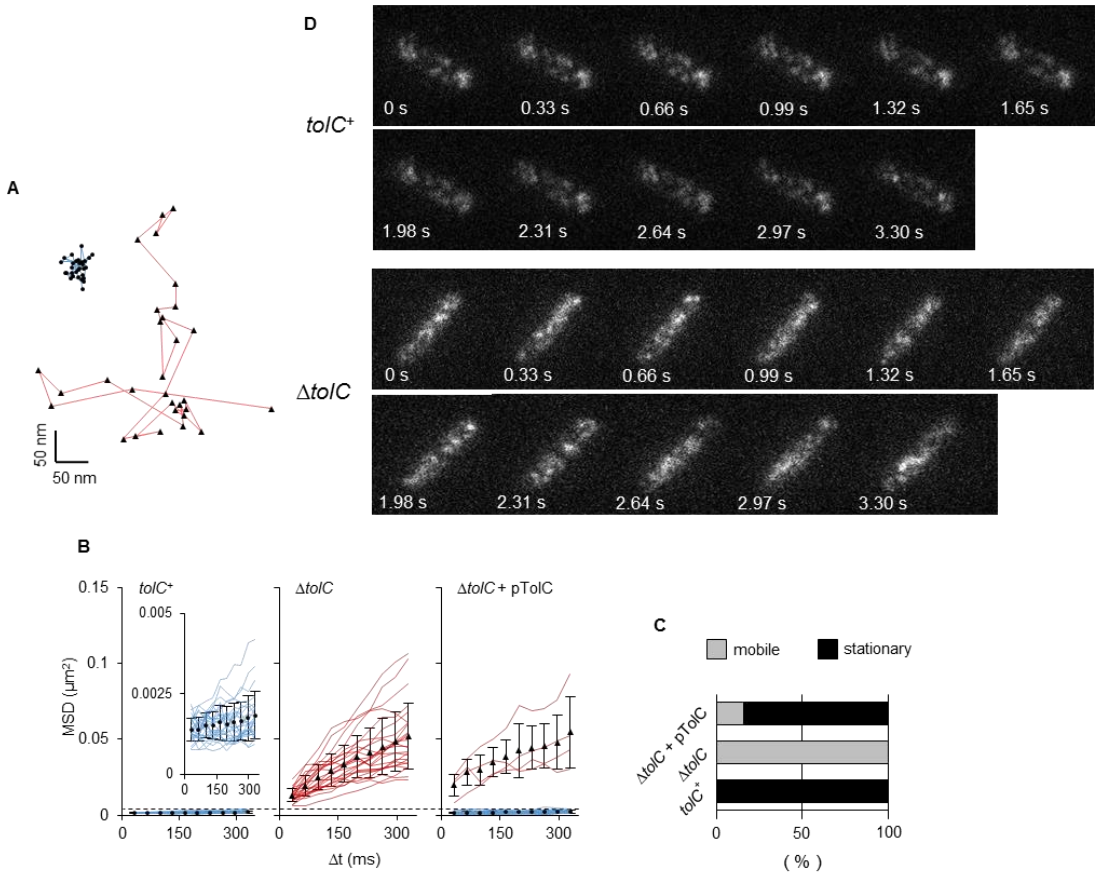

Fig. II-5. AcrB-GFP dynamics in the cytoplasmic membrane.

(A, B, C, D) x-y trajectories of AcrB-GFP in YKN12 (blue line) and YKN17 (red line) with the TIRF illumination (A) and time lapse images (D), MSD-Δ*t* plots of AcrB-GFP foci (B) and fractions of mobile and stationary AcrB-GFP foci (C) in the presence or absence of TolC. Fluorescent foci were traced and their MSDs were calculated (*n* = 25). Closed symbols with error bars indicate averaged MSD values of all mobile (triangles) or stationary (circles) trajectories at each time with standard deviations. Dotted line in panel B indicates the boundary MSD value at time 330 ms to define mobile (red lines) and stationary foci (blue lines).

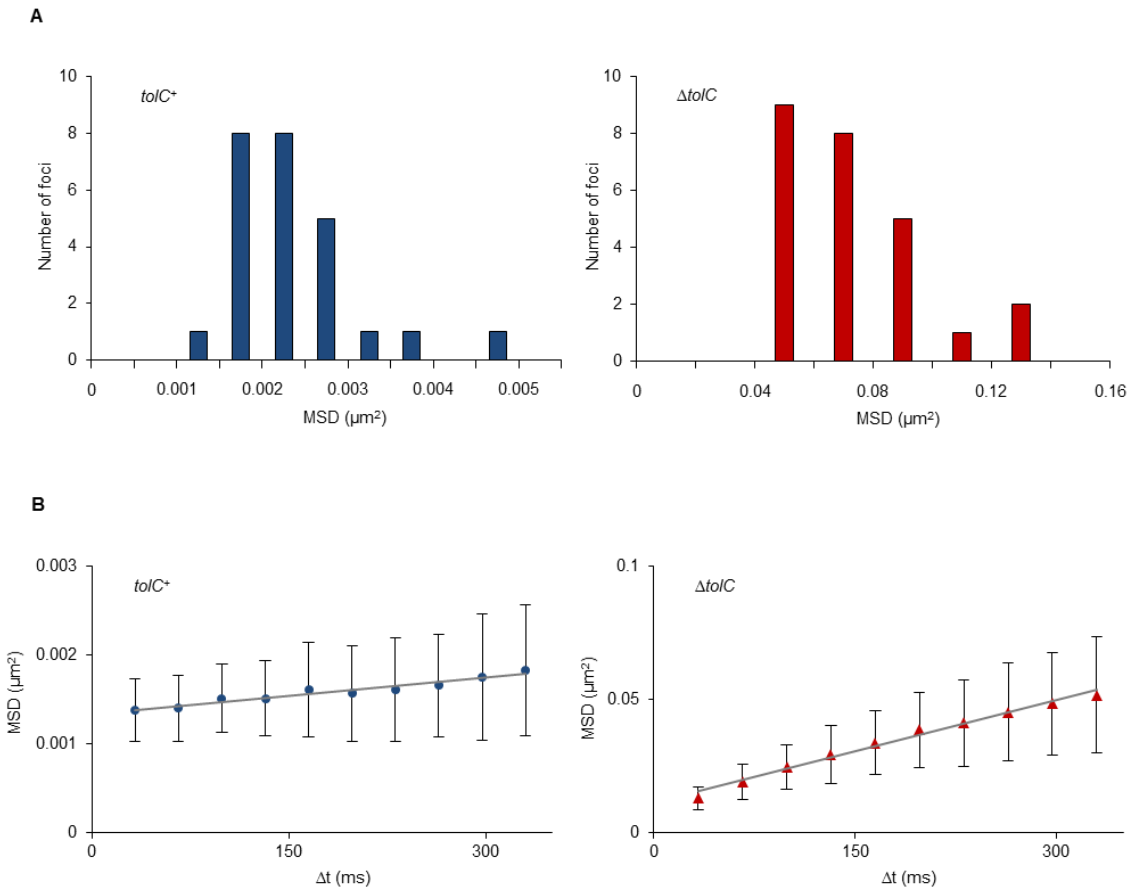

Fig. II-6. Tracking AcrB-GFP foci and calculation of their mean square displacements (MSD) in strains YKN12 and YKN17.

(A) Distribution of MSD at time 330 ms of AcrB-GFP foci in the presence (left) or absence (right) of TolC. (n = 25). (B) The averaged MSD-Δt plots for stationary (left) and mobile (right) fractions of AcrB-GFP. These data were fitted with linear regressions.

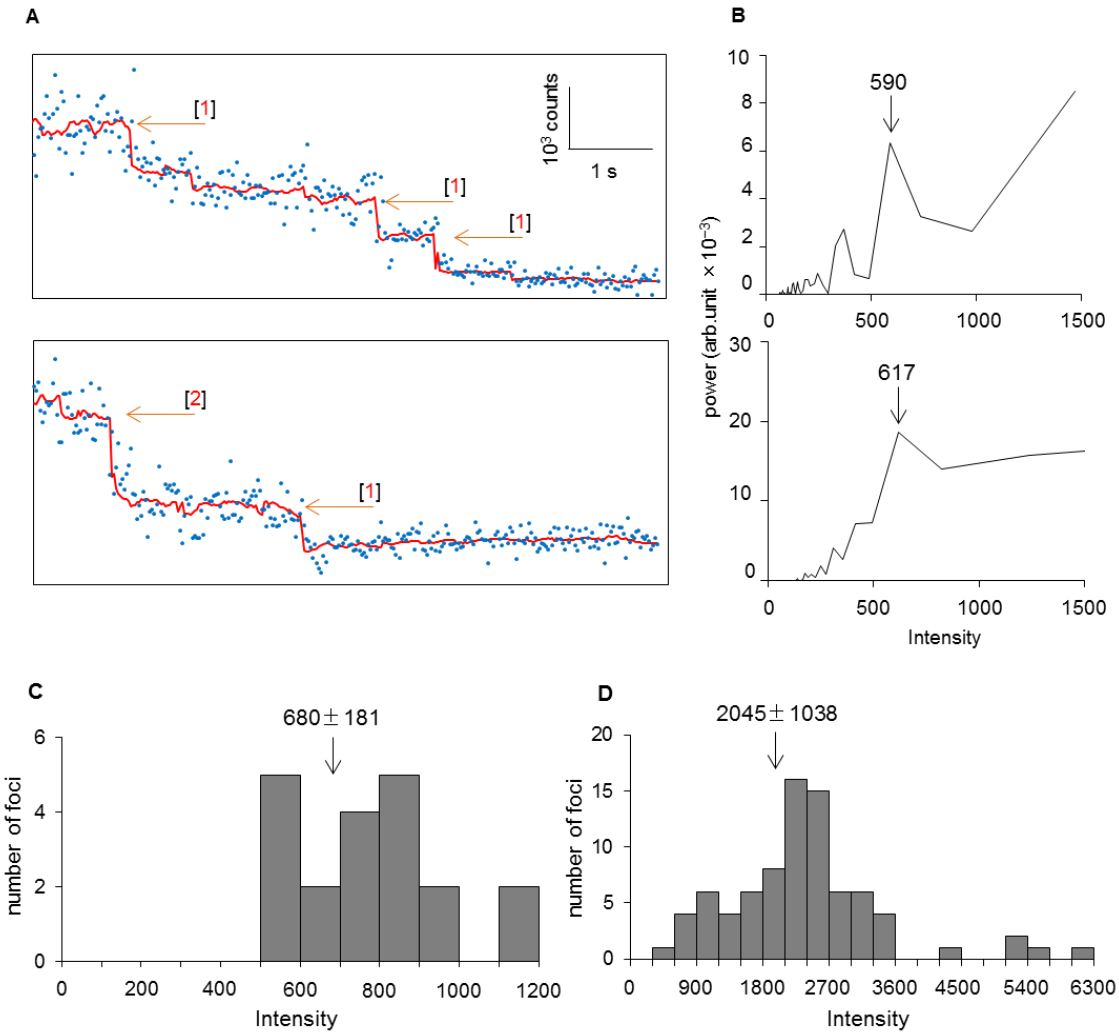

Fig. II-7. Trimeric nature of fixed AcrB-GFP foci in the presence of TolC.

(A) Three-step photobleaching of a single AcrB-GFP focus. Blue dots, the intensity of AcrB-GFP per frame; red line, output of the edge-detecting filtered intensity (window = 15); orange arrows, the positions of predicted steps with measured a step size respectively; and red numbers, the number of bleached GFP molecules. (B) Power spectra of the PDDF with arrows indicating step sizes of photobleaching trace. (C) Distribution of the detected step sizes of photobleaching (n = 20). Arrow indicates an average (mean ± S.D.) of the step sizes. (D) Distribution of the fluorescence intensity of single foci at the first frame obtained by subtracting the background value (n = 81). Arrow indicates an average (mean ± S.D.) of the foci intensity.

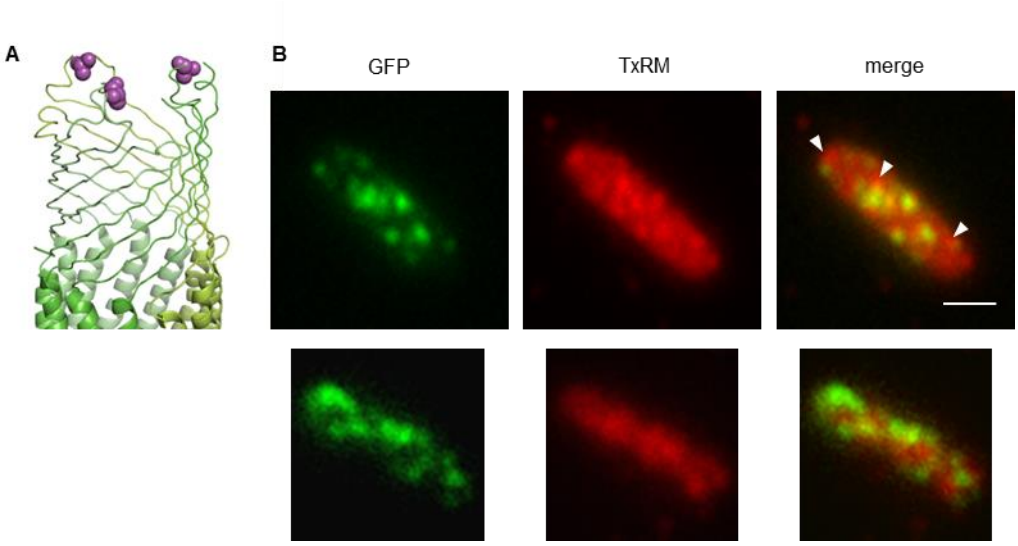

Fig. II-8. The co-localization of AcrB-GFP foci with fluorescently labeled TolC.

(A) The crystal structure of the extracellular loop of the TolC trimer (PDB ID code: 2XMN). Purple balls indicate the positions of A269C. (B) Co-localization of AcrB and TolC. Images of AcrB-GFP (left) and TxRM-labeled TolC-A269C (middle) were merged (right). Arrow heads indicate TolC-A269C foci that did not co-localize with AcrB-GFP (top). Observation of TxRM-treated cells expressing AcrB-GFP and wild-type TolC. YKN17 cells transformed with plasmid pKRB2100 (wild-type TolC) were grown in the presence of arabinose and treated with 1 μM TxRM. Images of the same fields taken with emission filters for GFP (left) or TxRM (middle) were merged (right) (bottom). Scale bar, 1 μm.

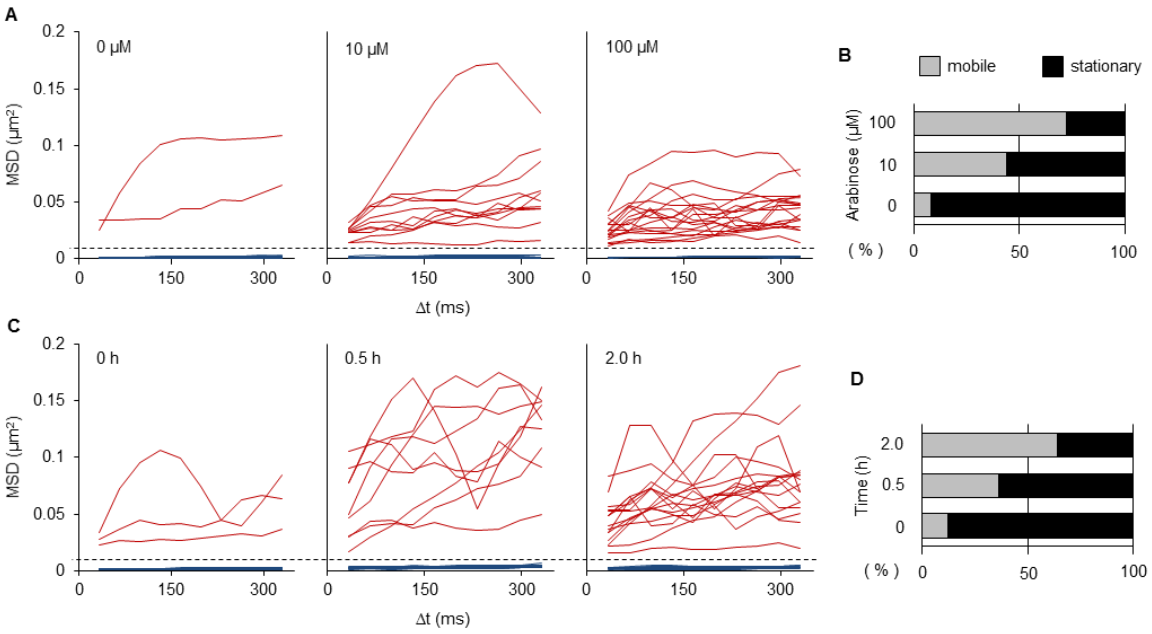

Fig. II-9. The AcrD expression influenced the mobility of AcrB-GFP foci.

Effect of plasmid-encoded AcrD induced with 0−100 μM arabinose for 2 h (n = 25) or with 100 μM arabinose for 0−2 h (n = 25). (A, C) MSD-Δt plots of AcrB-GFP foci under various conditions. Dotted line indicates the boundary MSD value at time 330 ms to define mobile (red lines) and stationary foci (blue lines). (B, D) Fractions of stationary and mobile AcrB-GFP foci.

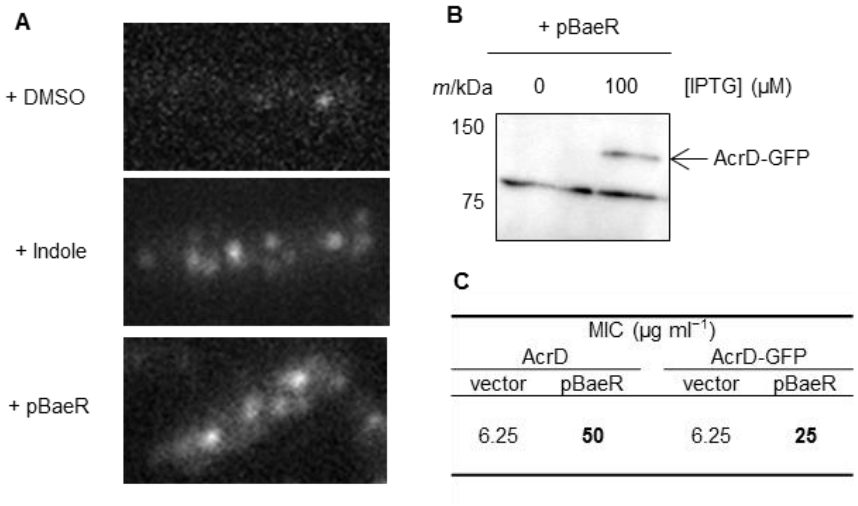

Fig. II-10. The expression and MIC test of AcrD-GFP.

TIRF observation (A) and immunodetection (B) of AcrD-GFP (*m*/kDa = 140) in MBRT02 cells. (C) Resistance of cells expressing AcrD (strain BW25113) or AcrD-GFP (strain MBRT02) to carbenicillin. Cells carrying the BaeR-expressing plasmid pBaeR or the vector pCA24N were cultured with 100 μM IPTG.

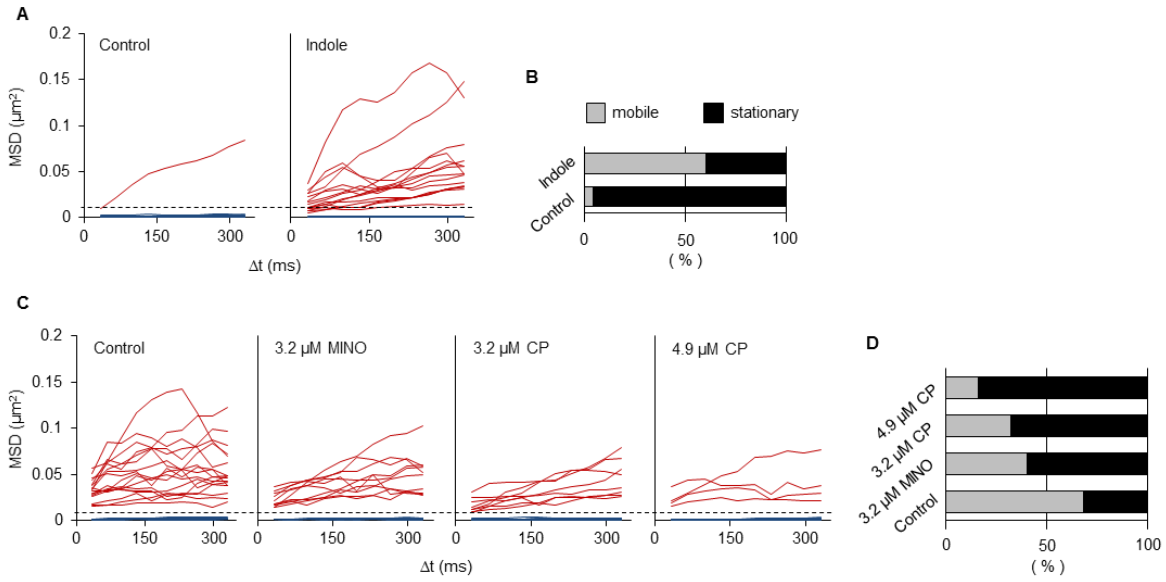

Fig. II-11. The effect of induction of the chromosomal *acrD* gene.

(A, B) Effect of induction of the chromosomal *acrD* gene. The native *acrD* gene was induced with 4 mM indole for 2 h (*n* = 25). Cells were also treated with 1% dimethyl sulfoxide as a negative control. (C, D) Effects of the AcrB-specific substrates chloramphenicol (CP, 4.9 or 3.2 μM) and minocycline (MINO, 3.2 μM) on MSDs of AcrB-GFP under AcrD-inducing conditions. The plasmid-borne *acrD* gene was induced with 100 μM arabinose for 2 h (*n* = 25). MSD-Δ*t* plots (A, C) and fractions of stationary and mobile of AcrB-GFP foci (B, D).

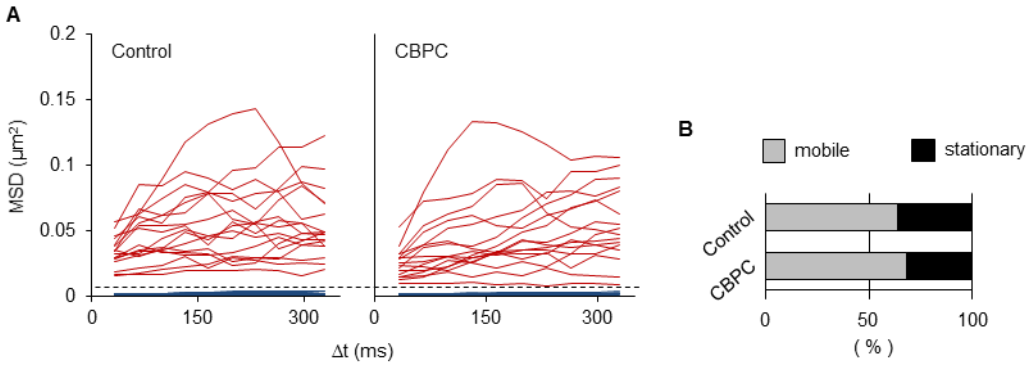

Fig. II-12. Effect of an AcrD-specific substrate on transporter exchange.

Carbenicillin (CBPC) was added to the culture for 1.5 h after *acrD* was induced with 100 μM arabinose. Cells were further incubated for 0.5 h. (A) MSD-Δ*t* plots of AcrB-GFP with (left) or without (right) 6.25 μM CBPC. (B) The fractions of stationary and mobile AcrB-GFP foci (n = 25) with or without CBPC.

Discussion

In this study, I examined dynamics and assembly of AcrB, the major RND-type xenobiotic efflux transporter in the inner membrane (IMT) of *E. coli*. With TIRF microscopy, I found that most foci of GFP-fused AcrB were stationary in the presence of TolC, whereas they showed lateral diffusion in the membrane of the Δ*tolC* strain. The co-localization of AcrB-GFP with TolC was detected by chemically labeling TolC. I also found that the induction of AcrD destabilizes the AcrBA-TolC complex, presumably resulting in the exchange of AcrB-GFP in the preexisting complex with newly synthesized AcrD. The fraction of mobile AcrB-GFP foci increased with increasing expression levels of AcrD. Furthermore, the AcrD-induced instability of the AcrBA-TolC complex was suppressed by AcrB-specific substrates, suggesting that the assembly of the RND-type efflux system is a regulated dynamic process.

The *D* value of moving AcrB-GFP obtained in our TIRF microscopic analyses ($3.5 \pm 1.8 \times 10^{-2}$ μm^2 s^{-1}) is roughly one order of magnitude smaller than that of the *E. coli* serine chemoreceptor Tsr fused to the fluorescent protein Venus ($4.0 \pm 0.1 \times 10^{-1}$ μm^2 s^{-1}) (Oh et al., 2014). The difference in the *D* value between these proteins is reasonable considering that in the number of TMs: AcrB is a homotrimer of 12-TM subunits and Tsr is a homodimer of 2-TM subunits (or exists as a trimer of dimer). The fact that AcrB-GFP foci are stationary in the presence of TolC is consistent with the structural feature of TolC. Because the periplasmic

extension of TolC penetrates the peptidoglycan layer, a rigid three-dimensional mesh-like supramolecule, the lateral diffusion of TolC molecules must be very restricted. Thus, the diffusion of AcrB, once assembled into the complex with TolC, must also be limited.

I detected three-step photobleaching of stationary AcrB-GFP foci. I also detected double-sized steps, indicating that two GFP molecules were bleached simultaneously or successively. These results demonstrate that at least a majority of TolC-associated AcrB molecules form trimers. The broad distribution of MSD value in the absence of TolC might reflect interactions with other membrane proteins or a mixed population of AcrB-GFP monomers and oligomers.

Leake et al (2006) reported that TIRF illumination visualizes approximately one sixth of the surface of a cell within 100 nm of a coverslip (Leake et al., 2006). In the *tolC*$^{+}$ strain, I detected an average of 7.5 ± 1.6 (mean ± S.D., n = 50) stationary foci of AcrB-GFP per cell in the TIRF illumination field. I therefore estimate that there are 45 ± 9.6 foci of AcrB-GFP trimers per cell, which corresponds to 135 ± 28.8 molecules of AcrB-GFP per cell if a majority of foci represented trimers. This estimation is consistent with estimated values the literature (< 500 molecules) (Tikhonova & Zgurskaya, 2004). Because the number of TolC molecules per cell is nearly three times higher than that of AcrB molecules (Tikhonova & Zgurskaya, 2004), and because the level of TolC expressed from the plasmid-borne gene must be higher than from the chromosomal gene, it is likely that not all labeled TolC co-localized

with AcrB-GFP and that TolC is in excess.

Expression of the *acrAB* operon is regulated by AcrR repressor and transcriptional activators such as MarR and SoxS (Ma et al., 1996; Perez et al., 2012; Watanabe & Doukyu, 2012). However, the operon is known to be "constitutively" expressed under laboratory conditions (Sulavik et al., 2001), whereas genes encoding other IMTs, including AcrD, of RND-type xenobiotic efflux systems are expressed at very low levels in *E. coli* and are induced by environmental stimuli such as indole-induced and other stresses on the cell envelope (Hirakawa et al., 2005; Raffa & Raivio, 2002). Because AcrD shares TolC and AcrA with AcrB, and assuming that the induction signal for AcrD (indole) does not significantly affect the cellular amounts of AcrB, AcrA and TolC, it was reasonable to ask whether AcrD can replace AcrB in the preformed AcrBA-TolC complex. Indeed, the expression of AcrD either from the chromosomal gene with the native promoter (induced by indole) or the promoter-less gene under the control of the *araBAD* promoter (induced by arabinose) increased lateral diffusion of AcrB-GFP, which was otherwise stationary in complex with TolC and AcrA. This AcrD-induced instability of the AcrBA-TolC complex, which may result in transporter exchange, would be part of adaptive drug resistance, an important bacterial responses to harmful substances. It should also be noted that transporter exchange may occur between different molecules of the same IMT: for instance, the AcrBA-TolC complex may undergo assembly and disassembly with some frequency. Thus, an RND-type xenobiotic

efflux complex is not rigid or fixed but allows association and dissociation of its components.

The next obvious question is whether the AcrD-induced instability of the AcrBA-TolC complex can be regulated. Our results indicate that there is some level of regulation: the AcrBA-TolC complex was stabilized by the AcrB-specific substrates. Of the two substrates tested, minocycline showed weaker effects, likely because it has a lower affinity for AcrB. Minocycline might also be sequestered because it chelates divalent metal ions in the medium (Leyden, 1985). These results suggest that the AcrBA-TolC complex is stabilized by substrate binding, slowing the exchange of AcrB with AcrD. The stabilization of a ternary complex when it is in action should be advantageous for bacterial survival. In particular, AcrB can transport the widest range of substrates among all xenobiotic transporters (Nishino & Yamaguchi, 2001a), including the bacterium's own metabolites or their derivatives such as fatty acids and bile salts (Ma et al., 1995). Interference with the activity of AcrB when cells are exposed to its substrate(s) would presumably have adverse effects on viability (Murakami & Yamaguchi, 2003). The AcrD-specific substrate, however, had little effect on the stability of the ternary complex. Thus, the presence of a substrate for a non-associated IMT may not necessarily accelerate destabilization of preexisting ternary complexes. Alternatively, a free IMT might not bind its substrate. A thermodynamics study suggests that, in the absence of substrate, AcrB forms a symmetric trimer, and that forced substrate binding to one protomer induces and stabilizes an asymmetric form of the AcrB

trimer (Yao et al., 2010). *In vivo*, an IMT might bind its substrate to become an asymmetric trimer only when it is in the ternary complex. The resulting asymmetric IMT trimer might stabilize the IMT-MFP-OMC ternary complex, making it resistant to transporter exchange. Alternatively, the AcrBA-TolC complex might be stabilized by some endogenous substrate(s). The AcrBA-TolC complex might also be stabilized by some endogenous substrate(s) (Fig. II-13).

In this chapter, the full data were published in *Scientific Reports* (Yamamoto et al., 2016).

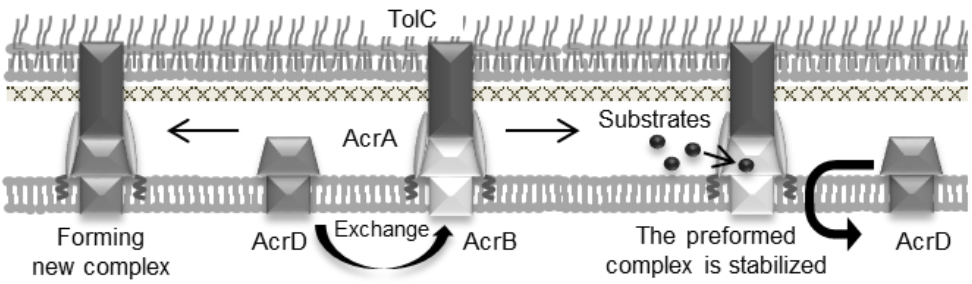

Fig. II-13. The transporter exchange model.

The pre-formed AcrB-AcrA-TolC complex becomes instable upon the induction of AcrD, which presumably result in the exchanges of AcrB with AcrD to form a new AcrDA-TolC complex (left). The pre-formed ternary complex can be stabilized by its substrates (right).

CHAPTER III

Accumulation of indole in the cell induces the multidrug efflux transporter gene *acrD*

Introduction

The RND-type multidrug efflux transporter AcrD is closely related to AcrB, and shares MFP AcrA and OMC TolC with AcrB (Aires & Nikaido, 2005). The AcrDA-TolC complex exports aminoglycosides and anionic β-lactams, such as carbenicillin and sulbenicillin, which are not transported by AcrB (Kobayashi et al., 2014; Nishino et al., 2003; Rosenberg et al., 2000). The *acrD* is expressed at very low levels in *E. coli* under the standard laboratory conditions and is induced upon the addition of indole to culture media via the TCS consisting of the sensor kinase BaeS and the response regulator BaeR (Hirakawa et al., 2005; Nishino et al., 2005). Indole is synthesized from tryptophan by a variety of bacterial species, including *E. coli*, and hence is present throughout natural environments (Lee & Lee, 2010).

This laboratory constructed a strain expressing GFP-fused AcrD from the chromosome of strain BW25113. In the resulting strain, fluorescence foci of AcrD-GFP were observed when cultured in the presence, but not in the absence, of 4 mM indole. Although the concentrations required for induction are consistent with the literature (Hirakawa et al., 2005), 4 mM seems too high compared to physiological concentrations of indole (0.6 – 1.2 mM; Li

& Young, 2013) which bacteria would encounter in the intestine (Knarreborg et al., 2002). Therefore, the real trigger or signal that a bacterium senses to induce AcrD must not be extracellular indole itself, but rather something resulting from high extracellular indole concentrations. Here, based on the following lines of evidence, I propose that it is intracellular indole that triggers the *acrD* expression. First, I observed fluorescent foci of AcrD-GFP in a *tolC*-deletion derivative strain, but not in the parental strain, without exposing to indole or any exogenous agents. The effect of the *tolC* deletion was reversed by the expression of wild-type TolC or mutant TolC defective in drug efflux. Second, the deletion of the tryptophanase gene *tnaA* or the TCS genes *baeSR* abolished the constitutive expression of AcrD-GFP in the *tolC*-deleted strain. Third, the direct measurements of indole concentration revealed that the intracellular concentration of indole in the *tolC*-deleted strain was higher than that in the *tolC*$^{+}$ strain.

Results

The deletion of *tolC* influences the *acrD* expression

I examined whether the expression of *acrD* is induced by the addition of indole as reported previously (Hirakawa et al., 2005). In strain MBRT02 which carries the chromosomal *acrD-gfp* gene (for detail, see CHAPTER II of this study), TIRFM observation detected AcrD-GFP foci when cells were treated with 4 mM indole for 2 h, but scarcely did

without indole (Fig. III-1A). Interestingly, in the *tolC*-deleted derivative strain MBRT05, AcrD-GFP foci were detected without treating with indole (Fig. III-1B, left). When complemented with a plasmid encoding TolC (pKRB2109), AcrD-GFP foci were not observed without indole (Fig. III-1B, middle). Furthermore, I constructed a *tnaA*-deleted derivative from MBRT05. In the resulting *tnaA tolC* double-deletion strain encoding AcrD-GFP (named YKN51), AcrD-GFP foci were not observed without indole despite the absence of TolC (Fig. III-1B, right). These results suggest that the deletion of *tolC* results in the constitutive expression of *acrD*.

I next measured the expression of AcrD-GFP quantitatively using a microplate reader. The fluorescence intensity of Δ*tolC* cells carrying the plasmid encoding TolC was decreased about 23%, compared to those with the empty vector (Fig. III-2A). The Δ*tolC* Δ*tnaA* double mutant showed decreased fluorescence intensity, which returned to the level of the parent strain by introducing a *tnaA*-expressing plasmid (Fig. III-2A, B). Moreover, the fluorescence intensity was substantially reduced by the deletion of *baeSR*, whose products mediate indole responses (Fig. III-2B). These results are consistent with the TIRFM observation of AcrD-GFP described above. Presumably, the deletion of *tolC* might causes the accumulation of indole, or some other factor, in the cytosol or some deformation in the cell surface, either of which might trigger the *acrD* expression by activating the BaeSR system.

The outer membrane channel TolC works as a part of RND efflux system with inner

membrane transporter. The constitutively expressed transporter AcrB and its paralog AcrF of *E. coli* are considered to play a central role in the efflux of intracellular xenobiotics. The deletion of *acrB* and *acrF*, however, had little effect on the AcrD-GFP expression (Fig. III-2B). I then asked whether TolC can complement the expression of AcrD-GFP without an interaction with transporters. Based on the literature (Tamura et al., 2005), I constructed a plasmid encoding mutant TolC with the substitution of a Gly×4 linker for residues Q142-A150 in the loop between helices H3 and H4 (named TolCΔloop), which is defective in drug efflux as judged from chloramphenicol resistance (Fig. III-2C). I also constructed a plasmid encoding TolC and TolCΔloop fused to mCherry (a red fluorescent protein). These fusion proteins were detected by immunoblotting with anti-RFP antibody without visible degradation products and apparently localized to the cell surface as judged from observation with epi illumination (Fig. III-2D, E). The expression of either mCherry-fused TolC or TolCΔloop AcrD-GFP in the *tolC*-deleted strain decreased the expression of AcrD-GFP (Fig. III-2A, C), suggesting that even mutant TolC defective in coupling to an inner membrane transporter can suppress the induction of *acrD*.

Measuring the amount of intracellular indole

I then examined whether indole is indeed accumulated in a Δ*tolC* cell using Kovac's reagent. About 33.5% difference was detected for the amount of intracellular indole between

in the *tolC*$^{+}$ (0.881 ± 0.199 × 10^{6} molecule/cell) and the *tolC*-deleted (2.629 ± 0.150 × 10^{6} molecule/cell) strain. It was estimated that the concentration of intracellular indole in a cell at 332.74 ± 75.27 μM and 992.45 ± 56.56 μM, respectively (Fig. III-3, right). In contrast, the difference of the amount of indole that was transported to the extracellular space was no more than about 5.6% (129.476 ± 1.381 × 10^{6} molecule/cell in the *tolC*$^{+}$ *vs* 122.637 ± 0.987 × 10^{6} molecule/cell in the Δ*tolC*). These values correspond to 167.76 ± 1.79 μM and 158.9 ± 1.28 μM, respectively. In the *tolC*-deleted strain, the total amount of indole was about 4.1% smaller than that in the *tolC*$^{+}$ strain. Moreover, when complemented with the TolC-encoding plasmid, the amount and concentration of indole returned to levels comparable to those of the parent strain. With TolCΔloop, the complementation level of any indole test was lower than those with wild-type TolC. These results suggest that the lack of TolC renders indole to be accumulated in the cell, which may induces the expression of *acrD*.

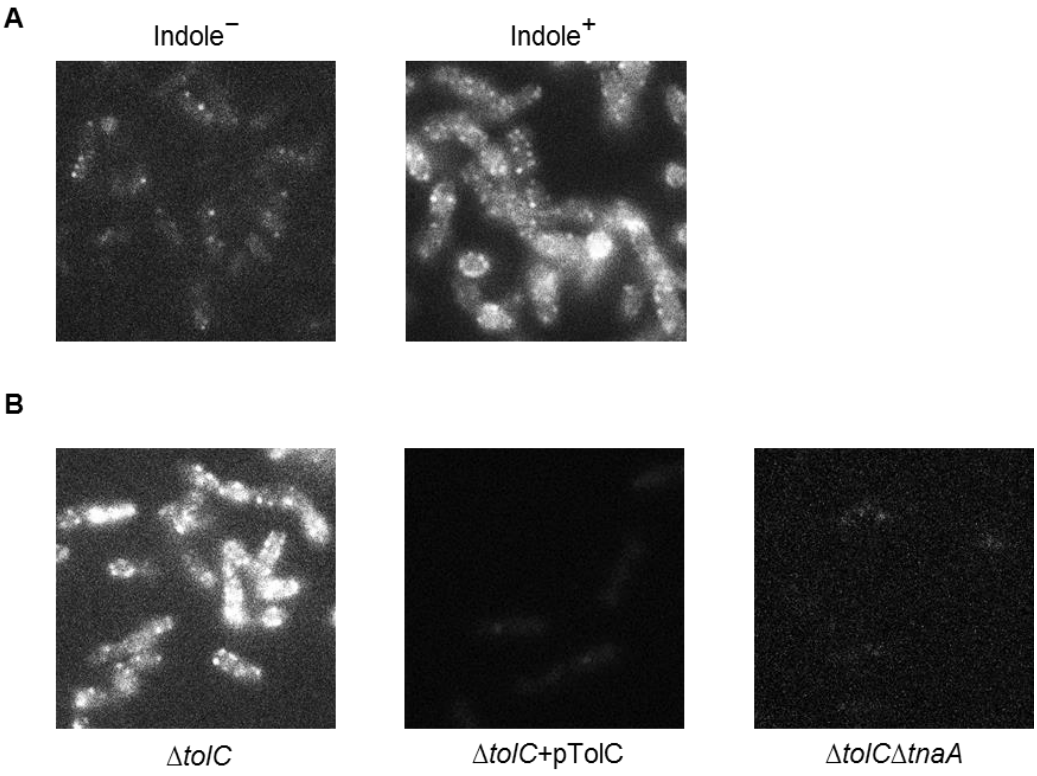

Fig. III-1. Observation of AcrD-GFP under various conditions.

Fluorescent imaging of AcrD-GFP from chromosomal gene with TIRFM. (A) In the presence of *tolC* strain MBRT02, cells were treated with or without 4 mM indole for 2 h. (B) Observation of AcrD-GFP in a *tolC*-deleted strain MBRT05 (left) and in a *tolC* and *tnaA*-deleted strain YKN51 (right). Cells carrying the TolC expressing plasmid pKRB2100 were cultured with 100 μM arabinose for 2 h (middle).

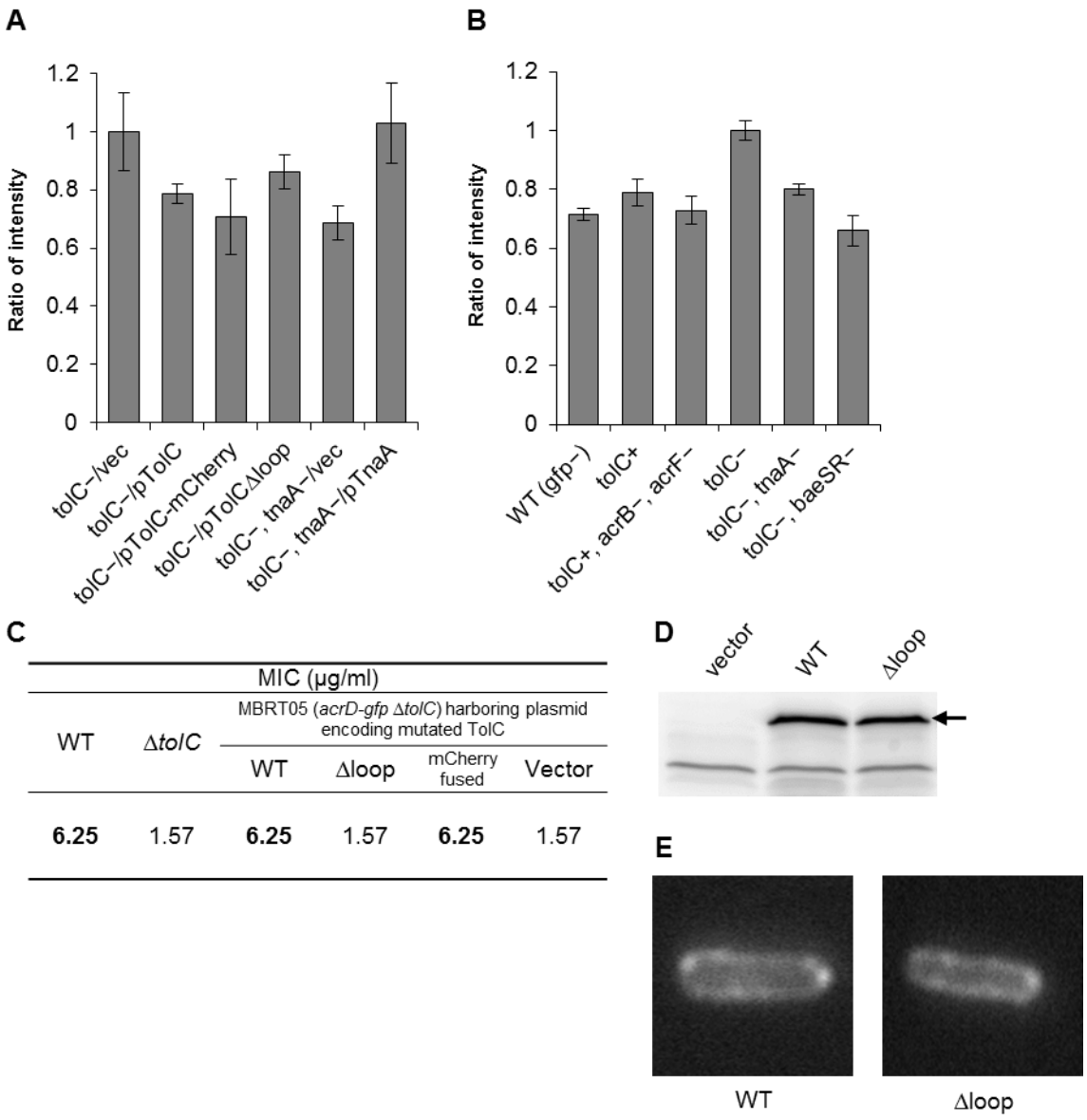

C

MIC (μg/ml)					
WT	Δ*tolC*	MBRT05 (*acrD-gfp* Δ*tolC*) harboring plasmid encoding mutated TolC			
		WT	Δloop	mCherry fused	Vector
6.25	1.57	**6.25**	1.57	**6.25**	1.57

Fig. III-2. The deletion of *tolC* induced the chromosome-encoded *acrD-gfp*.

(A, B) The relative of AcrD-GFP intensity in the various backgrounds using microplate reader. Each bar represents the mean ± standard deviation of data (n = 3). (A) Cells carrying the wild-type TolC, TolCΔloop mutant, mCherry fused TolC or TnaA-expressing plasmid or the vector pBAD24 were cultured with 100 μM arabinose. (C) Antibiotic susceptibility analysis. The *tolC*$^{+}$ (WT) and Δ*tolC* cells expressing AcrD-GFP from the chromosomal genes. The plasmid-encoded wild-type TolC and its variants were expressed in the Δ*tolC* strain. (D, E) The immunodetection (D) and epi fluorescent imaging (E) of mCherry fused TolC and TolCΔloop (m/kDa = 80) in the Δ*tolC* strain.

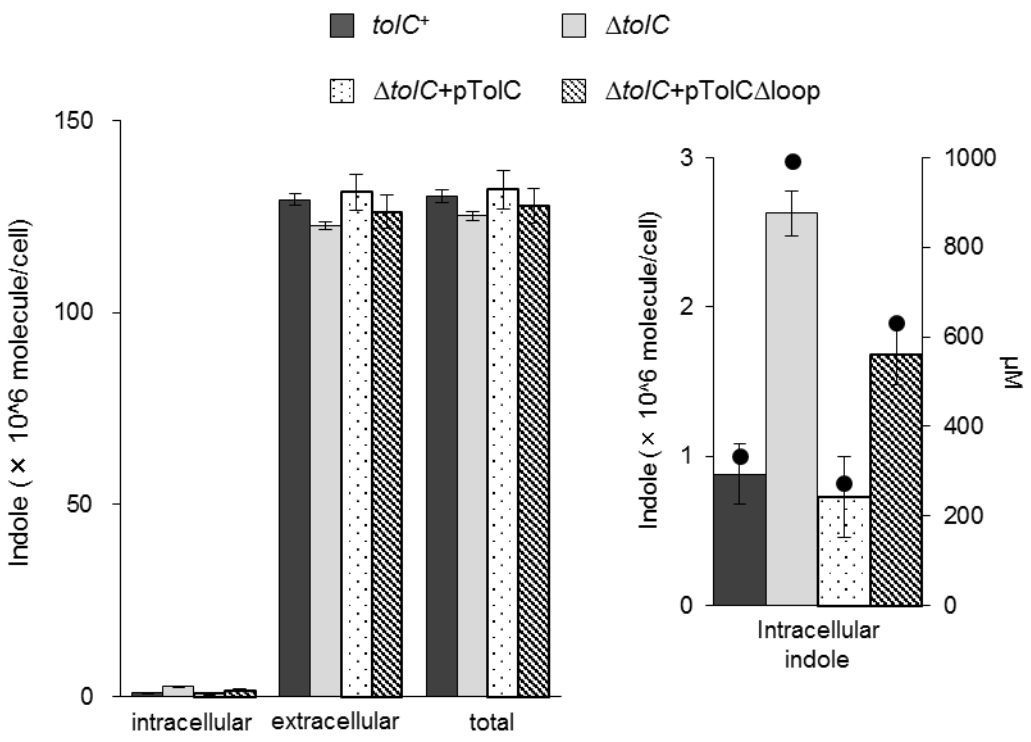

Fig. III-3. The measuring intra- and extracellular indole.

Cells carrying the wild-type TolC or TolCΔloop mutant-expressing plasmid or the vector pBAD24 were cultured with 100 μM arabinose. The amount of indole are shown as the accumulation of intracellular indole (intracellular), the excretion of indole to supernatant (extracellular), and the total amount of indole that have been produced by a cell (total) per cell (left). The closed circle indicates the concentration of intracellular indole (right). Each bar represents the mean ± standard deviation of data (n = 3).

Discussion

In this chapter, I examined whether the outer membrane channel TolC of RND-type transports indole to out of cells. With fluorescence microscopic observation, I found that a deletion of *tolC* induced the chromosome-encoded *acrD-gfp* without exogenous agents as indole. Because this induction was inhibited by the deficiency of tryptophanase TnaA which synthesizes indole from tryptophan, I suspected an increasing concentration of intracellular indole in the absence of *tolC*. Hirakawa et al reported that the expression of *acrD* is induced by the addition of indole to culture media via the TCS consisting of the sensor kinase BaeS and the response regulator BaeR (Hirakawa et al., 2005). Indeed the lacking BaeSR regulation system suppressed the expression of *acrD-gfp* in the *tolC*-deleted background, which was complemented with plasmid encoding BaeSR (Yamazaki, unpublished). These results reinforced that the intracellular indole induces the *acrD-gfp* expression via BaeSR.

In Kawamura-Sato et al, they proposed that AcrEF-TolC of RND-system involves in indole efflux based on there was about 1.7 times difference in the intracellular indole concentration between the *acrEF* mutant and wild-type strain (Kawamura-Sato et al., 1999). On the other hand, Pinero-Fernandez's group argued using by measuring concentration of supernatant indole that the excretion of indole is a free diffusion without support of RND-efflux system or other protein to transport indole (Pinero-Fernandez et al., 2011). Although, it is not clear from this literature whether RND-system affects the concentration of

intracellular indole. Then, I found that there was about 3 times difference in the amount of intracellular indole per cell between in the presence (330 μM) and the absence of TolC (990 μM). I thought that the reason why I had a difference of the estimated indole concentration with Kawamura-Sato et al is that they did not subtract a background quantity of the *tnaA*-deleted strain which produces no indole from an actual measurement (see materials and methods). In contrast, based on the amount of extracellular indole, it appears that TolC had little effect on indole excretion. The final extracellular indole concentration is dependent on the excretion of indole which is biosynthesized in early exponential phase (Kobayashi et al., 2006). Thus, these integrated extracellular indole concentration may counteract the effect of indole efflux by TolC. A high pH condition increases the concentration of extracellular indole as a result of inducing the expression of *tnaA* (Blankenhorn et al., 1999; Wyeth, 1919). It also has been reported that TolC may play a physiological role in pH homeostasis through an interaction with the proton motive force in a multidrug efflux transporter (Deininger et al., 2011). In the *tolC*-deleted strain, the total amount of indole which was produced by one cell was smaller than that in the *tolC*$^{+}$ strain. I suspected that this result reflects the difference in the amount of indole due to a change in the intracellular pH homeostasis with the loss of proton transfer by RND efflux systems.

The deletion of major RND-type inner membrane transporter AcrB and its paralog AcrF did not affect the AcrD-GFP expression, which raise the next obvious question whether

the interaction with TolC and inner membrane transporter involves in indole efflux. In fact, TolCΔloop mutant, which has no drug efflux activity, decreased the concentration of intracellular indole. These results suggested that TolC can transport indole to out of cell without an interaction with inner membrane transporter. TolC is the pore-like outer membrane channel whose entrance conformation is changed the closing-state into the opening-state by interaction with inner membrane transporter. However, non-interaction TolC state has been unclear in *vivo*. It is possible that indole directly passes through TolC whichever its state is switched.

The high concentration of extracellular indole (about 2 mM) induces the expression of multidrug transporter genes including *acrD* (Hirakawa et al., 2005). However, *E. coli* produces up to about 0.6 mM indole, which mainly depends on the concentration of tryptophan, in a rich medium including 0.5 mM tryptophan. The concentration of indole reaches about 4.5 mM at 24 h if the 5 mM tryptophan is ever added to the culture medium (Li & Young, 2013). In the intestine of pig, the maximum indole concentration has been estimated to be 0.12 mM with about <0.5-0.7 mM (in the small intestine) and <0.1 mM (in the large intestine) tryptophan (Knarreborg et al., 2002). Thus, it is unthinkable that the extracellular indole reaches up to 2 mM under normal physiological conditions. It was suggested that *E. coli* senses the change of indole concentration in not the supernatant but the cytosol. In my additional considerations, the possibility still remains that *E. coli* senses not only the indole

but also the envelope stress of its accumulation. An envelope stress by indole affects the expression of various gene including multidrug efflux gene *acrD* via TCS BaeSR and CpxAR in *E. coli* (Hirakawa et al., 2005; Raffa & Raivio, 2002). In fact, it have been known that a high concentration of indole, which is toxic to *E. coli*, influences the persister cell formation (Vega et al., 2012). The major envelope sensor CpxA might sense injurious stimuli of inner membrane that was induced by intracellular indole, and it transmits this signal to the cognate response regulator CpxR or BaeR as a cross-talk. In the complex web of indole signal pathway, my results suggested that indole-induced gene expressions are caused by intracellular indole signals (Fig. III-4).

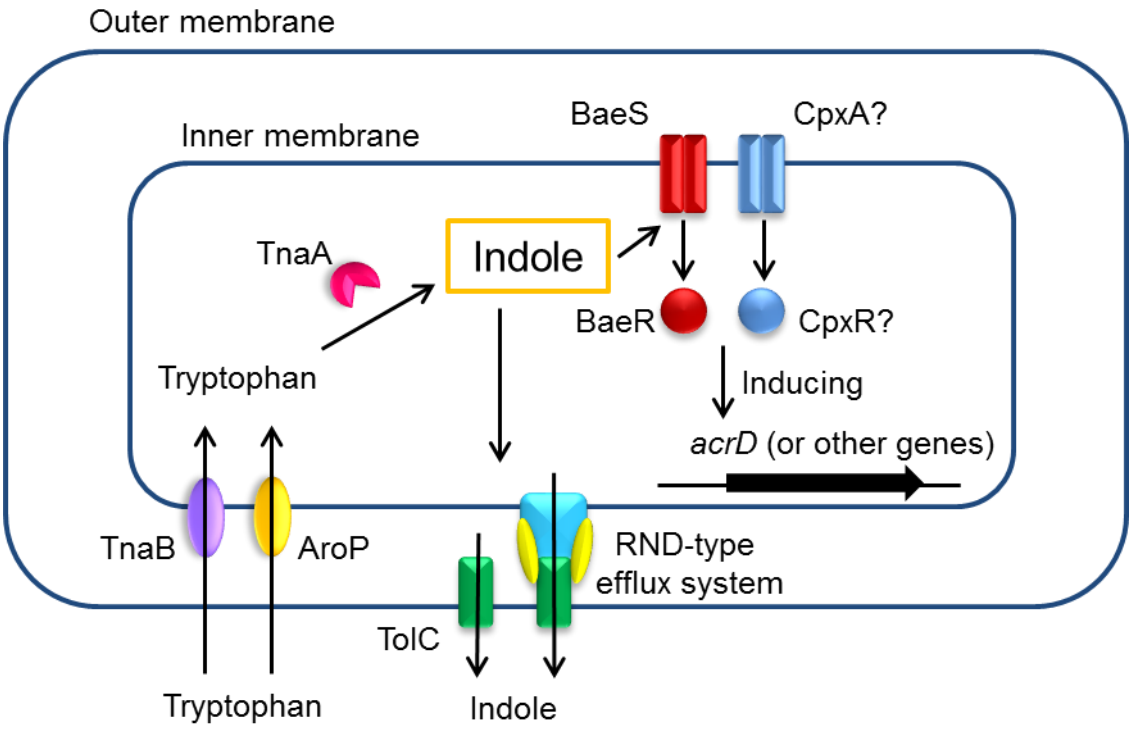

Fig. III-4. Proposed model of the gene expression by indole stimuli.

In this study, I proposed that the expression of *acrD* is caused by the accumulation of intracellular indole via two-component regulatory system. Arrows indicate transport or stimulus or induction.

CHAPTER IV

Methods for fluorometric imaging of outer and inner membrane proteins

Introduction

In cell biology, the fluorescent protein labeling techniques often are used for visualization of the organisms and protein complexes. These techniques can analyze localizations and dynamic of structures which are not detected in a live cell by the optical microscopy unmounting the fluorometric imaging systems. Moreover the fluorescent tag imaging do not require an immobilization like an immunostaining and the transmission or scanning electron microscopy methods. Although fluorescent protein fusion is critically useful, it potentially could cause artificial distributions. The fluorescent proteins have large molecular mass (e.g. GFP; 27 kDa) and some tags potentially dimerize, which inhibit the functions of fused protein (Swulius & Jensen, 2012). I also have tested the imaging using other florescent labeling methods.

The outer membrane channel TolC was stained by fluorescent reagent Texas Red maleimide in CHAPTER II. Because the N-terminus and C-terminus ends of TolC, which interact with membrane fusion protein AcrA, locate in periplasmic space, it is difficult to fuse TolC and fluorescent protein. I therefore tagged TolC with a tetracysteine (TC)-tag at its C-termini and examined their localization by staining with fluorescein arsenical hairpin binder–ethanedithiol (FlAsH-EDT_2) (Griffin et al., 1998; Hoffmann et al., 2010). FlAsH

specifically binds to a short peptide sequence of Cys-Cys-Pro-Gly-Cys-Cys (TC-tag), and it forms intermolecular disulfide linker (about 1.5 kDa). I also observed TC-tag fused histidine kinase CheA1 for the chemotactic signal transduction in *Vibrio cholerae* under aerobic and anaerobic conditions.

The amino acid chemoreceptor Mlp37 of *V. cholerae* was found to serve for taurine as well as serine, arginine and other amino acids. I determined the crystal structures of the ligand binding domain of Mlp37 in complex with L-serine and taurine. The structure revealed the slightly open conformation of the ligand binding domain in the serine complex. These findings led me to visualize Mlp37 *in vivo* with a fluorescently labeled amino acid: L-serine 5(6)-carboxyfluorescein ester (Ser-FAM), in which carboxyfluorescein is linked to the hydroxyl group of L-serine through an ester bond.

Results

Labeling of outer membrane channel TolC and CheA1 with FlAsH.

I constructed the plasmids, which are arabinose inducible vector, encoding C-terminal TC-tag fusion of TolC (TolC-TC) and wild-type TolC. In a *tolC*-deleted strain JW5503, fluorescence microscopic observation detected their localized foci of lateral regions of cell membrane expressing TolC-TC with any concentration of arabinose by fluorescent reagent FlAsH (Fig. IV-1A top). Huge foci were detected to a cell pole with 30 and 100 μM

arabinose (Fig. IV-1A bottom). These foci might be aggregated TolC trimers. However no foci were observed in cells expressing wild-type *tolC*, demonstrating that non-specific labeling was ignorable. The TolC-TC protein retained almost full activity as judged by the minimal inhibitory concentrations (MIC) of nalidixic acid (Fig. IV-1B).

Next I observed the localization of GFP-fused histidine kinase CheA1 of *V. cholerae* with or without sodium azide (NaN_3) that inhibits cytochrome *c* oxydase. Cells expressing CheA1-GFP at late logarithmic phase were incubated. The localization of CheA1-GFP foci were dispersed throughout the cell. NaN_3 dramatically altered the localization of CheA1-GFP foci, which showed the localization to a cell pole and lateral region of the membrane (Fig. IV-2 top). Moreover I also constructed TC-tag-fused CheA1 and observed their localization in the same as above conditions. These localization patterns were similar to those of CheA1-GFP (Fig. IV-2 bottom). These localization results of CheA1 including other chemotaxis-related proteins were published in *Molecular Microbiology* (Hiremath et al., 2015).

Observation of Mlp37 with a fluorescently labeled serine.

In *mlp24* and *mlp37*-double deleted strain Vmlp201, fluorescent spots were detected at poles of cells expressing wild-type *mlp37* from plasmid (pMlp37) with Ser-FAM (Fig. IV-3C) treating, but not those carrying empty vector (Fig. IV-3A). I also examined foci of Ser-FAM under the other ligands. A 10-fold molar excess of L-serine or taurine was added

when cells were exposed to Ser-FAM, which decreased the occurrence of polar foci. By contrast, adding L-glutamate, one of the weakest attractants, did not affect Ser-FAM labeling (Fig. IV-3A). These results suggest that the former attractants and Ser-FAM compete for binding to Mlp37. Moreover I constructed a plasmid encoding Mlp37-TagRFP (named pKRB116). When cells expressing the TagRFP-fused Mlp37 were treated Ser-FAM, florescence microscopy detected foci of Ser-FAM, which co-localized with Mlp37-TagRFP (Fig. IV-3B). These results not only confirm the mechanism of ligand recognition by Mlp37, but also provide, for the first time, a tool to visualize ligand binding to a bacterial chemoreceptor *in vivo*.

A

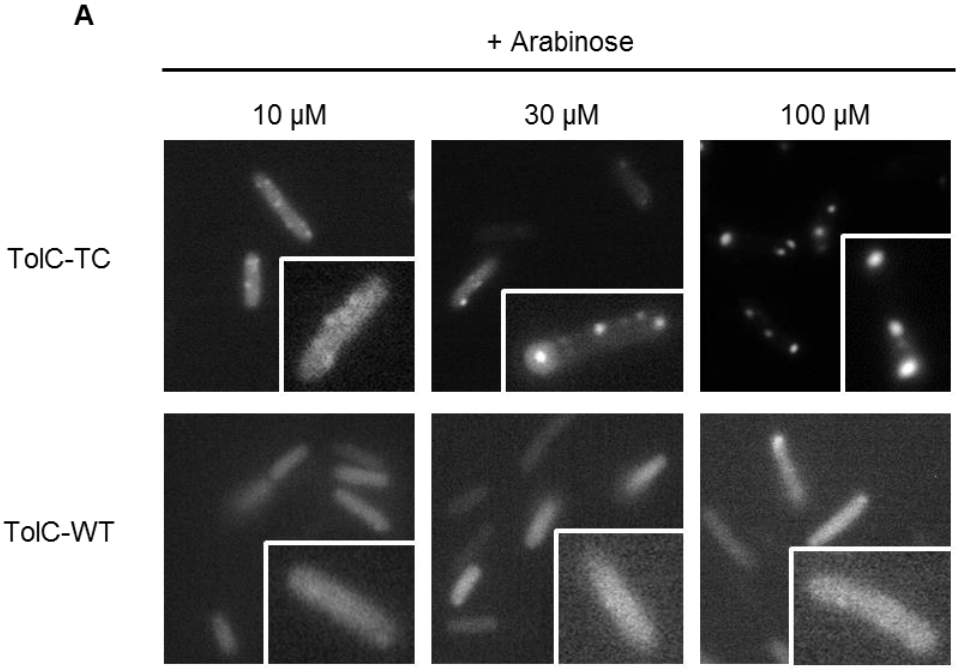

B

MIC (μg·ml^{-1})		
vector	TolC-WT	TolC-TC
0.78	**3.13**	**3.13**

Fig. IV-1. FlAsH stained images of cells expressing TolC-TC.

Cells carrying the TolC-TC expressing plasmid pKRB2107 or the TolC expressing plasmid pKRB2100 in a *tolC*-deleted strain JW5503 were cultured with 10−100 μM arabinose for 2 h. (A) Fluorescent imaging of TolC-TC and wild-type TolC with FlAsH. (B) Antibiotic susceptibility analysis. Bold face represents the resistance indicative of the significant efflux activity.

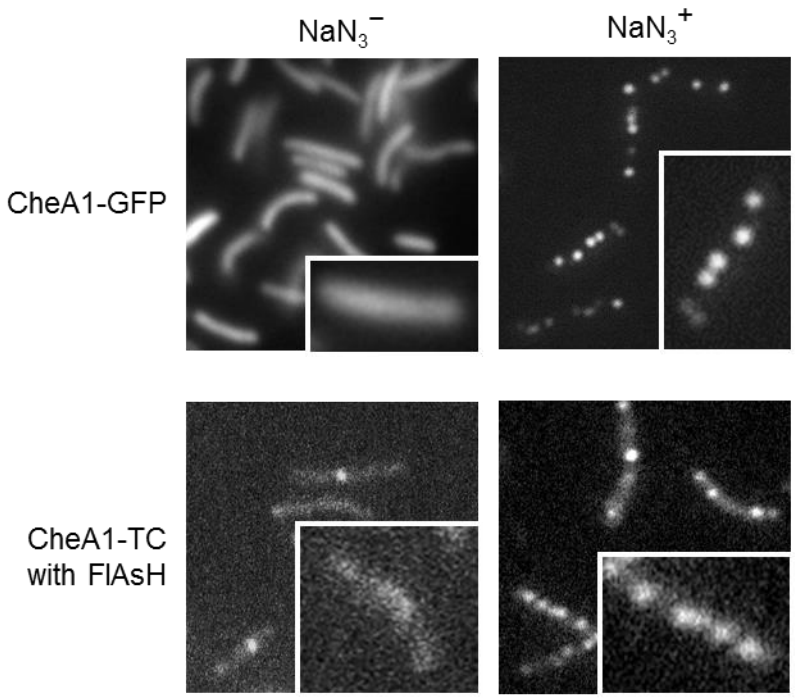

Fig. IV-2. Effect of NaN_3 on the localization of CheA1.

Fluorescent imaging of CheA1-GFP and FlAsH labeled CheA1-TC in O395N1 strain. Cells carrying the CheA1-GFP expressing plasmid pAH191 or the CheA1-TC expressing plasmid pKRB101 with or without NaN_3.

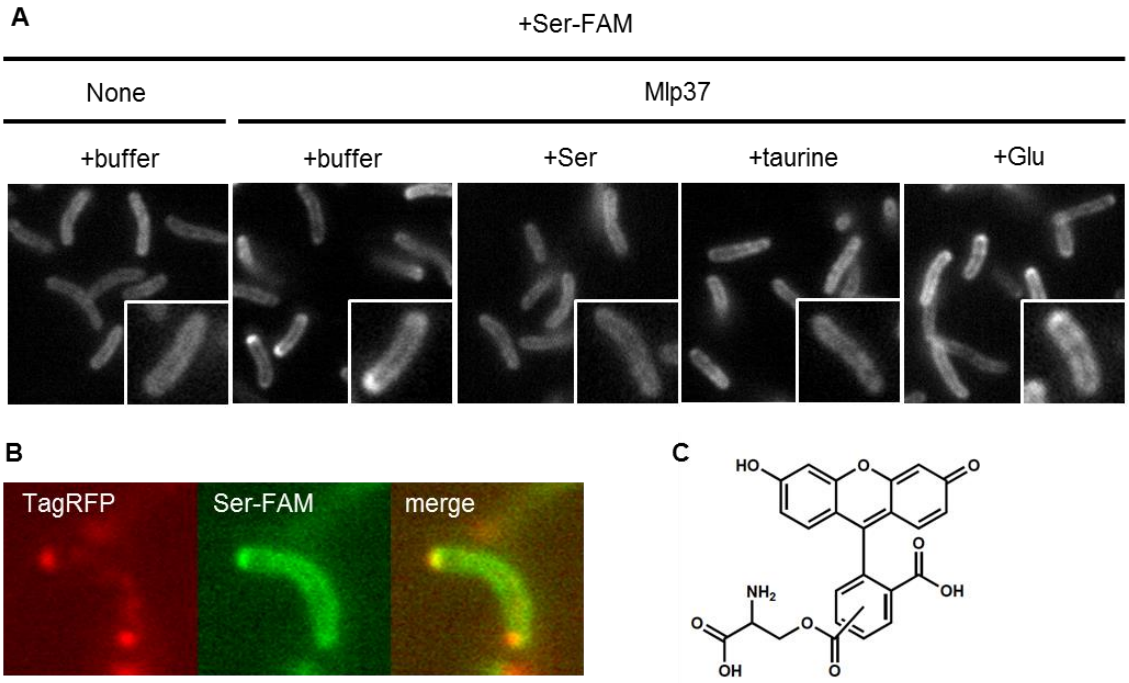

Fig. IV-3. Fluorescent imaging of Mlp37 with Ser-FAM.

(A) Competitive labeling of Mlp37 with carboxyfluorescein-labeled L-serine (Ser-FAM). Vmlp201 (Δ*mlp24* Δ*mlp37*) cells carrying the pAH901 vector (none) or pMlp37 (Mlp37) were incubated in TMN buffer containing 100 μM Ser-FAM supplemented with none (+ none), 1 mM serine (+ Ser), 1 mM taurine (+ taurine), or 1 mM glutamate (+ Glu). (B) Co-localization of Ser-FAM with Mlp37. Vmlp201 cells expressing Mlp37-TagRFP were treated with Ser-FAM: left, Mlp37-TagRFP; middle, Ser-FAM; right, merge. (C) Ser-FAM structural formula.

Discussion

In CHAPTER II, labeling of TolC was performed with substituting Cys for Ala-269 and staining by the thiol-reactive fluorescent reagent Texas Red maleimide (TxRM). However the high background fluorescence was shown, which was caused by non-specific labeling of other Cys-containing proteins, in spite of staining at low concentrations for a short period of time. In this chapter, I explored the methods of TolC staining with higher specificity and no effect on the efflux activity for *in vivo* live-cell imaging. FlAsH-EDT_2 is formed non-fluorescent complex with ethanedithiol (EDT). When it binds to TC-tag amino acids sequence, these FlAsH-TC complex becomes fluorescent. This property achieves a low background fluorescence. TolC-TC fusion protein retained a full function of drug efflux, and their foci localized to lateral region of the cell membrane. However some large foci were detected to a cell pole in an over expression of TolC-TC (30 and 100 μM arabinose), which may be caused by the disulfide bonds with each other's Cys of TC-tags. The localization of GFP-fused CheA1 of *V. cholerae* depends on aerobic condition in the culture. These behavior of CheA1 are consistent with those of the GFP fusion and TC-tag fusion. The effects of aerobic conditions suggest that the characteristic localization of System I components must be triggered neither by growth retardation nor by mechanical stimuli but by impaired energy metabolism (Hiremath et al., 2015). The FlAsH labeling is helpful as a *in vivo* live-cell imaging method with low background and low harmful influence to its function alternative to

fluorescent proteins.

The observation of the chemoreceptor is usually performed with direct visualizing using fluorescent protein or specific reagent *in vivo*. In this study, I observed a fluorescein linked ligand binding to the chemoreceptor. Serine is one of the strongest attractants of the chemoreceptor Mlp37 of *V. cholerae*. Mlp37 was labeled with Ser-FAM, which can be outcompeted by excess amounts of serine or taurine, validates the structural information. It also provides a cell biological tool to study bacterial chemotaxis, which has not been available for study of *E. coli* or any other bacterium until now.

In this chapter, the full data about localization of CheA1 and Mlp37 were published in in *Molecular Microbiology* (Hiremath et al., 2015), and were accepted to *Scientific Reports* (Nishiyama et al., 2016).

CHAPTER V

Conclusions

The RND-type efflux system of bacteria plays a major role in multidrug resistance, and it has been studied particularly for its structure and function such as transporter's substrates. However, it has been unclear how RND-ternary complex was assembled and the regulations of the expression of RND components genes under the physiological condition. In this thesis, I aimed to understand how the newly synthesized molecules assemble into ternary complex and how indole as a cellular signal molecule acts as expression of *acrD* gene.

In CHAPTER II of this study, I focused on the subcellular dynamics of inner membrane transporter AcrB, and tried visualization of the construction processes of the efflux protein complex. TIRFM observation detected that the fraction of moving AcrB-GFP foci increased with increasing levels of the closely related transporter AcrD (named "transporter exchange"). Moreover, I demonstrated that this exchange was suppressed by AcrB-specific substrates. I propose that newly synthesized transporter molecules can destabilize preexisting RND-type efflux complexes to facilitate transporter exchange. This exchange is suppressed by substrates of the transporter that is already in the complex. This mechanism may enable a rapid adaptive resistance to a newly encountered toxic compound. Increasing the instability of the RND-type efflux complex could facilitate the development of effective cocktails of

antibiotics that are substrates for different drug efflux systems to overcome drug resistance by gram-negative bacteria. In CHAPTER III of this study, I focused on indole efflux by RND-systems and the expression of indole-induced gene *acrD*. First, I focused on the data of lacking of TolC induced the expression of *acrD*. Measuring the intracellular concentration of indole, I demonstrated that TolC involves in indole efflux. Second, TolC mutant whose drug efflux activity was inactivated which decreased the concentration of intracellular indole. This results suggested that TolC is able to transport indole to extracellular environment without an interaction with inner membrane transporter. I proposed that the expression of *acrD* is caused by the accumulation of intracellular indole via two-component regulatory system BaeSR, and also *E. coli* senses not only direct stimulus of indole but also the envelope stress by indole accumulation.

In CHAPTER IV of this study, I examined the cellular protein imaging using FlAsH labeling methods and fluorescent amino acid serine alternative to fluorescent protein. TC-tag-fused proteins were labeled and localized without loss of original functions. This method established high specificity labeling and low background fluorescence in live cell. The method using fluorescent serine (Ser-FAM) is novel approach of visualizing chemoreceptor directly.

CHAPTER VI

Materials and Methods

Strains and plasmids

Bacterial strains and plasmids used in this study are described in Table VI-1, 2. The plasmid vector pTrcHisB (Invitrogen) carries the *trc* promoter, *lacI*^{q} and *bla*. The pTrcHisB-derived plasmid pDS1050 encodes Gly_3−linked−GFP (Hiremath et al., 2015). The plasmid vectors pBAD24 and pBAD33 carry *bla* and *cat*, respectively, in addition to the *araBAD* promoter and *araC*, which encodes the regulator of the *araBAD* promoter (Guzman et al., 1995). The plasmid pTWV228 is a pBR322-based vector carry *bla* and *lac* promoter (Takara Bio). The primers used for the plasmid and the strain constructions in this study are described in Table VI-3.

Construction of plasmids encoding wild-type or GFP-fused IMT.

The *acrB*- or *acrD*-coding region was amplified using PCR to introduce *Nhe*I and *Bgl*II sites at their 5′ and 3′ ends, respectively. The resulting fragment was cloned between the *Nhe*I and *Bgl*II sites of the vector pDS1050 to yield plasmids encoding AcrB-GFP (pKRB2000) or AcrD-GFP (pKRB2010). For tight regulation of *acrD* expression, plasmid pBAD24 was used as a vector to clone a PCR-amplified coding region with *Nco*I and *Hin*dIII

sites at its 5′ and 3′ ends, respectively, to yield pKRB2050. The 3.3-kb *Mlu*I-*Hin*dIII fragment of pKRB2050 was cloned between the corresponding sites of plasmid pBAD33 to yield pKRB2053.

Construction of plasmids encoding wild-type or mutant TolC.

A *tolC*-expressing plasmid was constructed by cloning a PCR-amplified fragment containing the 5′-untranslated and the coding regions of *tolC* between the *Sac*I and *Hin*dIII sites of the vector pBAD33 to yield plasmid pKRB2100 encoding wild-type TolC. The upstream primer used was designed to cover 28 bases just upstream of the deduced Shine-Dalgarno sequence of chromosomal *tolC*: 5′−CGAGCTCTTGATCGCGCTAAATACTGCTTCACCAC−3′ (the double underlined sequence represents the *Sac*I recognition site). And also a *tolC*-expressing plasmid was constructed by a PCR-amplified fragment was cloned between the *Nhe*I and *Hin*dIII sites of vector pBAD24 to yield plasmid pKRB2109 encoding wild-type TolC. A derivative of pKRB2100 encoding TolC-A269C (pKRB2104) was constructed using the QuickChange II one-day site-directed mutagenesis method (Stratagene) with Pyrobest DNA Polymerase (Takara Bio) and *Dpn*I (New England Biolabs). A derivative of pKRB2109 and pRE1300 (Tamai, 2013) encoding TolCΔloop (pKRB2123) and mCherry-fused TolCΔloop (pKRB2122) was constructed by TolC substituting Gly×4 linker for Q142-A150 in the loop between H3

and H4 helix. A tetracysteine (TC; Cys-Cys-Pro-Gly-Cys-Cys) tagged *tolC*-expressing plasmid was constructed by inserting TC sequence in between A269 and A270 (pKRB2107).

Construction of plasmid encoding TnaA.

The *tnaA*-expressing plasmid was constructed by a PCR-amplified fragment was cloned between the *Nhe*I and *Hin*dIII sites of vector pBAD24 to yield plasmid pKRB803 encoding TnaA.

Construction of plasmid encoding TC-tagged CheA1.

For TC-tagged CheA1, its gene was amplified using primers containing a sequence for a 3 × Gly linker followed by a C-terminal TC-tag and were cloned into the plasmid vector pTrcHisB (pKRB101).

Construction of plasmid encoding TagRFP fused Mlp37.

For construction of a plasmid encoding Mlp37-TagRFP, the TagRFP coding region was amplified by standard PCR using plasmid pTagRFP-C (Evrogen) as a template with primers designed for cloning and introducing a 3 × Gly linker at the N-terminus of TagRFP. The amplified fragment was cloned into plasmid pTWV228 (Takara Bio) to yield pKRB112 expressing free TagRFP with the linker. The *mlp37* gene was amplified using pMlp37 as a

template and was cloned into plasmid pKRB112 to yield pKRB116 expressing the Mlp37-TagRFP fusion.

Construction of strains YKN12 and MBRT02 with chromosome-encoded AcrB-GFP and AcrD-GFP, respectively.

Strains were constructed using a λ Red recombination system with plasmid pKD46 encoding the Red recombinase (Datsenko & Wanner, 2000) and positive selection for the loss of tetracycline resistance (Bochner et al., 1980). To replace the stop codon of *acrB* or *acrD* on the chromosome of the standard strain BW25113 with the selectable tetracycline-resistance gene (*tetRA*), I designed primers with 40-nucleotide arms and generated fragments using PCR with plasmid pKRB2000 or pKRB2010 as the template. After recombination, selection and isolation, *tetRA* was replaced by a Gly_3-GFP-encoding fragment with 40-nucleotide arms at their 5′ and 3′ ends. Tetracycline-sensitive clones were selected using tetracycline-sensitive medium (1% Bacto Tryptone, 0.5% Yeast Extract, 1% NaCl, 0.2% glucose, 50 μg mL^{-1} chlortetracycline hydrochloride, 1% NaH_2PO_4-H_2O, 12 μg mL^{-1} fusaric acid, and 0.1 mM zinc chloride).

Construction of the *tolC, tnaA* and *acrF*-deletion strain.

These genes deletion strains were introduced using P1 transduction with strains

JW5503 (Baba et al., 2006) JW3686 and JW3234 as donors, and YKN12, MBRT05k$^-$ and MBRT04k$^-$ as recipients, respectively. After the selection on LB medium containing kanamycin and sodium citrate, transductants were purified twice. These strains were named YKN17, YKN51 and YKN58, respectively.

Removing kanamycin cassette.

The plasmid pCP20 encoding FLP recombinase is a temperature-sensitive replication (Datsenko & Wanner, 2000). Constructed kanamycin-resistant mutants were transformed with pCP20 to yield ampicillin-resistance were selected at 30°C for 18 h. Transformants were colony-purified at 43°C for 16 h in a damp. Then, these were tested for loss of an ampicillin-resistance and kanamycin-resistance.

Construction of the *baeSR*-deletion strain YKN37.

Strain was constructed using a λ Red recombination system with plasmid pKD46 encoding the Red recombinase (Datsenko & Wanner, 2000). To replace the target gene on the chromosome of the strain MBRT05 with the tetracycline-resistance gene (*tetRA*) including 40-nucleotide arms.

Analyses of single molecule behaviors using TIRF microscopy.

Cells were grown in TG medium [1% Bacto Tryptone, 0.5% NaCl and 0.5% (w/v) glycerol] supplemented with appropriate antibiotics with shaking at 30°C for 16 h. The overnight cultures were diluted 100-fold into fresh TG medium and incubation was continued for 4 h. Cells were harvested and washed twice with MLM buffer (10 mM potassium phosphate buffer pH7.0, 0.1 mM potassium EDTA pH7.0, 10 mM sodium lactate pH7.0 and 0.01 mM L-methionine).

The expression of AcrD-GFP or AcrD form the chromosomal gene was induced by the addition of indole or introduction of a plasmid encoding BaeR (pCA24N-baeR, pBaeR) (Kitagawa et al., 2005). Cells were grown in TG medium supplemented with appropriate antibiotics with shaking at 30°C for 16 h. The culture was diluted 100-fold into fresh TG medium and further cultured for 2 h, and then 1% DMSO (negative control), 4 mM indole or 100 μM isopropylthiogalactoside (IPTG) were added to the culture, which was then incubated for 2 h. Cells were harvested and washed twice with MLM buffer.

Experiments to test the stability of the ternary complex were conducted using plasmid pKRB2050 carrying the wild-type *acrD* coding region downstream of the arabinose-inducible *araBAD* promoter. YKN12 cells (*acrB-gfp*) transformed with pKRB2050 were grown for 16 h with shaking at 30°C in TG medium supplemented with ampicillin. Cultures were diluted 100-fold into fresh TG medium and cultured for another 2 h. Arabinose at appropriate concentrations was then added to the culture and incubation continued for

another 2 h. The *tolC* complementation test was performed with induction of the plasmid-borne *tolC* at 100 μM arabinose. Cells (Δ*tolC*) transformed by plasmid pKRB2100 were harvested and washed twice with MLM buffer. When necessary, antibiotics were added at appropriate concentrations 1.5 h after the addition of arabinose.

Cells were spotted onto a poly-L-lysine-coated coverslip, washed with MLM buffer and were observed using objective-type TIRF microscopy (Sako et al., 2000; Tokunaga et al., 1997) with an Olympus IX71 equipped with a 100× oil-immersion objective lens, lasers and a dichroic mirror (Semrock Di01-R488-561). GFP was visualized using a Cobolt Blues 50 mW laser (Cobolt 0473-04-01-0050-300) and emission filter (Semrock FF01-520/35-25). TxRM was visualized using a Cobolt Jive 50 mW laser (Cobolt 0561-04-01-0050-300) and emission filter (Semrock FF01-593/40-25). Images were recorded with 33 ms exposure using an EMCCD camera (Andor iXon DU-897). All of the image analysis was performed with the ImageJ ver. 1.48 software (NIH) and custom LabVIEW programs. For tracking single foci, each images were filtered with the rolling ball algorithm (*Rolling Ball Radius*: 12 pixels) to subtract the background intensity. I defined a 7 × 7 pixel (350 × 350 nm) region of interest (ROI) centered on a focus in the first frame of the images with the threshold appropriately adjusted (Leake et al., 2006). Individual foci were tracked through >30 frames. The mean square displacements (MSDs) were calculated as described in the literature (Kusumi et al., 1993). The diffusion coefficients (=*D*) were calculated from the values of averaged MSD-Δ*t*

plots with linear regressions fitting of the first ten points.

Estimation of the number of AcrB-GFP molecules per focus using three-step photobleaching.

The analysis was carried out essentially as described in the literature (Leake et al., 2006). In images recorded with the exposure times of 33 ms for 10 s using TIRF microscopy, fluorescent intensity per frame of a ROI centered at a fluorescent focus was monitored over time. The edge-detecting method of non-linear filtering (window = 15) was used to identify photobleaching steps in the time-course of fluorescence intensity of AcrB-GFP foci (Leake et al., 2006; Smith, 1998).

Fluorescent labeling of TolC-A269C.

YKN17 cells (Δ*tolC*) transformed with plasmid pKRB2100 encoding TolC-A269C or the vector pBAD33 (a negative control) were grown in TG medium at 30°C for 16 h. The culture was diluted 100-fold into fresh TG medium and cultured for 2 h, and then 10 μM arabinose were added to the culture, which was further incubated for 2 h. Washed cells were treated with 1 μM TxRM (Texas Red C_2 Maleimide, Molecular Probes) at room temperature for 5 s and then quickly washed twice with MLM before observation by TIRF microscopy. Images were averaged (10 frames) using the ImageJ ver. 1.48 software (NIH) with custom

macros.

Antibiotic susceptibility analysis.

Minimum inhibitory concentrations (MICs) were determined on YT agar plates (0.8% Bacto Tryptone, 0.5% Yeast Extract, 0.5% NaCl, 1.5% Bacto Agar) containing chloramphenicol, nalidixic acid, or carbenicillin at various concentrations. When necessary, 100 µM arabinose or 100 µM IPTG were added. YT agar plates were made using 2-fold serial dilutions techniques (Nishino & Yamaguchi, 2001a). Bacteria were grown in YT medium at 37°C for 16 h. The culture was diluted 100-fold into fresh YT medium supplemented with 100 µM arabinose or 100 µM IPTG, if necessary, and cultured further. YT agar plates with antibiotics and appropriate inducers, if necessary, were inoculated with aliquots of cell suspension (2.5 µL each containing 10^5 cells) and then incubated at 37°C for 18 h.

Immunoblotting.

Cells were grown in TG medium supplemented with appropriate antibiotics with shaking at 30°C for 16 h. The overnight culture was diluted 100-fold into fresh TG medium and further cultured for 4 h. Cells were harvested, washed twice with MLM buffer, resuspended in MLM with 8.3% 2-mercaptoethanol and 16.7% SDS, and subjected to SDS-PAGE followed by immunoblotting using a monoclonal anti-GFP antibody (Nacalai

Tesque) and anti-TagRFP antibody (Evrogen). Immune complexes were detected using horseradish-peroxidase (HRP)-labeled anti-mouse IgG (KPL) and the Immobilon Western Chemiluminescent HRP Substrate system (Merck Millipore).

FlAsH labeling of TC-tagged proteins.

FlAsH staining was carried out according to the original protocols (Griffin et al., 1998; Hoffmann et al., 2010) with modifications. Cells were grown at 30˚C in TG medium with appropriate antibiotic. Overnight cultures were diluted 50-fold into fresh TG medium and incubated for 4 h at 30˚C (TolC) or 37˚C (CheA1). Cells were harvested by centrifugation at room temperature and resuspended in 100 µl of MLM or TMN buffer [50 mM Tris-HCl (pH-7.4), 5 mM glucose, 100 mM NaCl] in *E. coli* or *V. chorea* strain, respectively. Ethanedithiol (EDT, Nacalai Tesque), tris-(2-carboxyethyl) phosphine (TCEP, Nacalai Tesque), and Lumio^{TM} Green (Invitrogen) were added to final concentrations of 0.25 mM, 1 mM and 0.5% (v/v), respectively. Cells were then incubated for 1 h at 30ºC, washed twice with MLM or TMN buffer and subjected to fluorescence microscope observations. NaN_3 (final concentration: 0.2%) was added to TMN buffer, if necessary. MAS-coated glass slides (Matsunami Glass Ind., Osaka) were used to immobilize cells. All images were recorded and processed by using a cooled charge-coupled-device camera ORCA-ERII (Hamamatsu Photonics) and the software Metamorph ver. 7.6 (Universal Imaging).

Ser-FAM labeling and the observation of TagRFP-fused Mlp37.

Cells carrying the pAH901 (Nishiyama et al., 2012) vector pMlp37 were grown at 30˚C in TG medium supplemented with 50 μg/ml ampicillin. Overnight cultures were diluted 50-fold into fresh TG medium and incubated for 4 h at 37˚C. Cells were harvested by centrifugation at room temperature and resuspended in 100 μl of TMN buffer and 100 μM Ser-FAM [L-serine 5(6)-carboxyfluorescein ester] (Eurofins Genomics Inc., Tokyo) was added. If necessary, non-labeled L-serine or taurine (final concentration: 1 mM) was added to TMN buffer. Cells were then incubated for 30 min at 37ºC, and washed once with TMN buffer. An aliquot of the cell suspension was spotted onto a MAS-coated glass slide (Matsunami Glass Inc., Osaka). Cells were then observed under a fluorescence microscope (Olympus IX71) equipped with a 100× oil-immersion objective lens. TagRFP-fused Mlp37 was visualized using fluorescence mirror units U-MWIG3 (Olympus). All images were recorded and processed by using a cooled charge-coupled-device camera ORCA-ERII (Hamamatsu Photonics) and the software Metamorph ver. 7.6 (Universal Imaging).

Observation of AcrD-GFP from chromosomal gene using TIRF microscopy.

Strain MBRT02, MBRT05 and YKN51 cells were grown in TG medium with shaking at 30°C for 16 h. The overnight cultures were diluted 50-fold into fresh TG medium

and incubation was continued for 4 h. When *acrD-gfp* was expressed by indole, the culture was diluted 50-fold into fresh TG medium and further cultured for 2 h, and then 1% DMSO (negative control), 4 mM indole were added to the culture, which was then incubated for 2 h.

The *tolC* and *tnaA* complementation tests were performed with induction of the plasmid-borne *tolC* (pKRB2109) and *tnaA* (pKRB803) at 100 μM arabinose. Cells were harvested and washed twice with MLM buffer. Cells were spotted onto a poly-L-lysine-coated coverslip, washed with MLM buffer and were observed using TIRF microscopy with an Olympus IX71 equipped with a 100× oil-immersion objective lens, lasers and a dichroic mirror (Semrock Di01-R488-561). AcrD-GFP was visualized using a Cobolt Blues 50 mW laser (Cobolt 0473-04-01-0050-300) and emission filter (Semrock FF01-520/35-25). Images were recorded with 33 ms exposure using an EMCCD camera (Andor iXon DU-897). All of the image analysis was performed with the ImageJ ver. 1.48 software (NIH).

Measuring intensity of AcrD-GFP

Cells were grown in TG medium with shaking at 30°C for 16 h. The overnight cultures were diluted 50-fold into fresh TG medium and incubation was continued for 4 h. The *tolC* and *tnaA* complementation tests were performed with induction of the plasmid-borne *tolC* (wild-type and its variants) and *tnaA* at 100 μM arabinose for 4 h. Cells were harvested and resuspended in 200 μl of MLM buffer. Cell samples were applied into

individual wells of a 96-well microplate (IWAKI 3860-096) and their intensity were measured at 490 nm excitation and 530 nm emission using microplate reader (CORONA MTP-880). These data were plotted on a chart based on the intensity in MBRT05 as a positive control.

Measuring indole production.

Measuring indole concentration was carried out according to the original protocols (Kawamura-Sato et al., 1999; Li & Young, 2013; Pinero-Fernandez et al., 2011) with modifications. Cells were grown in TG medium with supplemented 50 μg/ml ampicillin with shaking at 30°C for 16 h. The overnight cultures were diluted 50-fold into fresh 15 ml of TG medium and incubation was continued for 4 h. The *tolC* complementation test was performed with induction of the plasmid-borne *tolC* (wild-type and its variants) at 100 μM arabinose for 4 h. Cells were harvested, and its supernatants were treated with a sterilizing filter (Merck Millipore Millex-GP 0.22 μm PES 33mm RS). For measuring the concentration of extracellular indole, the 500 μl of sterilized supernatants were added 300 μl of Kovac's reagent (Merck Millipore) and were incubated for 5 min at room temperature. Then, for measuring the concentration of intracellular indole, the cell pellets were dissolved by 500 μl of kovac's reagent and were incubated for 5 min at room temperature. A 50 μl portion of upper surface of reacted sample was diluted in 950 μl of 1-butanol. The absorbance at 540 nm was measured by the spectrophotometer (GE Healthcare), and indole concentration was

calculated using a standard curve.

Table. VI-1. Bacterial strains used in this study.

	Relevant characteristics	Parent	Source or reference
E. coli strains			
BW25113	wild type	W1485	Datsenko & Wanner, 2000
JW0451	Δ*acrB*::*kan*	BW25113	Baba *et al*., 2006
JW3234	Δ*acrF*::*kan*	BW25113	Baba *et al*., 2006
JW3686	Δ*tnaA*::*kan*	BW25113	Baba *et al*., 2006
JW5503	Δ*tolC*::*kan*	BW25113	Baba *et al*., 2006
YKN12	*acrB-gfp*	BW25113	Yamamoto *et al.*, 2016
YKN17	*acrB-gfp* Δ*tolC*::*kan*	BW25113	Yamamoto *et al.*, 2016
MBRT02	*acrD-gfp*	BW25113	Yamamoto *et al.*, 2016
MBRT04	*acrD-gfp* Δ*acrB*::*kan*	BW25113	Tamai, 2013
MBRT04k^{-}	*acrD-gfp* Δ*acrB*	BW25113	This study
MBRT05	*acrD-gfp* Δ*tolC*::*kan*	BW25113	Tamai, 2013
MBRT05k^{-}	*acrD-gfp* Δ*tolC*	BW25113	This study
YKN37	*acrD-gfp* Δ*tolC*::*kan* Δ*baeSR*::*tetRA*	BW25113	This study
YKN51	*acrD-gfp* Δ*tolC* Δ*tnaA*::*kan*	BW25113	This study
YKN58	*acrD-gfp* Δ*acrB* Δ*acrF*::*kan*	BW25113	This study
V. cholera strains			
O395N1	chemotaxis wild type	O395	Hiremath *et al.*, 2015
Vmlp201	Δ*mlp24* Δ*mlp37*	O395N1	Nishiyama *et al.*, 2016

Table. VI-2. Vectors and plasmids used in this study.

	Relevant characteristics	Parent	Source or reference
pTrcHisB	vector	–	Invitrogen
pAH191	CheA1-GFP	pTrcHisB	Nishiyama *et al.*, 2016
pDS1050	GFP fusion vector plasmid (C-terminal)	pTrcHisB	Hiremath *et al.*, 2015
pKRB101	TC-tagged CheA1	pTrcHisB	Nishiyama *et al.*, 2016
pKRB2000	AcrB-GFP	pTrcHisB	Yamamoto *et al.*, 2016
pKRB2010	AcrD-GFP	pTrcHisB	Yamamoto *et al.*, 2016
pBAD24	vector	–	Guzman *et al.*, 1995
pKRB803	TnaA	pBAD24	This study
pKRB2050	AcrD	pBAD24	Yamamoto *et al.*, 2016
pKRB2109	TolC	pBAD24	This study
pKRB2122	mCherry-fused TolCΔloop	pBAD24	This study
pKRB2123	TolCΔloop	pBAD24	This study
pRE1300	mCherry-fused TolC	pBAD24	Tamai, 2013
pBAD33	vector	–	Guzman *et al.*, 1995
pKRB2053	AcrD	pBAD33	Yamamoto *et al.*, 2016
pKRB2100	TolC	pBAD33	Yamamoto *et al.*, 2016
pKRB2104	TolC-A269C	pBAD33	Yamamoto *et al.*, 2016
pKRB2107	TC-tagged TolC	pBAD33	This study
pTWV228	vector	–	Takara Bio
pAH901	carrying FLAG-tag	pTWV228	Nishiyama *et al.*, 2012
pMlp37	FLAG-tagged Mlp37	pTWV228	Nishiyama *et al.*, 2016
pKRB112	TagRFP fusion vector plasmid	pTWV228	Nishiyama *et al.*, 2016
pKRB116	TagRFP-fused Mlp37	pTWV228	Nishiyama *et al.*, 2016
pKD46	λ Red recombinase	–	Datsenko & Wanner, 2000
pCP20	FLP recombinase	–	Datsenko & Wanner, 2000
pCA24N	vector carrying His-tag	–	Kitagawa *et al.*, 2005
pBaeR	His6-BaeR	pCA24N	Kitagawa *et al.*, 2005

Table. VI-3. Primers used in this study.

Products	Sequence
pKRB2000	ctagctagcatgcctaatttc
	gaagatctatgatgatcgacag
pKRB2010	cagttaatgtaatgcctcctac
	caccacggtatattgtttccg
	ctagctagcatggcgaatttc
	gaagatctttccgggcgcggcttc
pKRB803	ctagctagcaggaggaattcaccatggaaaactttaaacatctccctgaaccg
	cccaagcttttaaacttctttaagttttgcggtgaagtgac
pKRB2050	catgccatggatggcgaatttctttattgatcgcccc
	cccaagcttttattccgggcgcggcttcag
pKRB2109	ctagctagcaggaggaattcaccatgaagaaattgctccccattcttatcggc
	cccaagctttcagttacggaaagggttatgaccgttac
pKRB2122	caaaccaccggcggaggcggaatcaccgacgtgcagaacgcccgc
	gtcggtgattccgcctccgccggtggtttgatctaattgacggtagatcgc
pKRB2123	caaaccaccggcggaggcggaatcaccgacgtgcagaacgcccgc
	gtcggtgattccgcctccgccggtggtttgatctaattgacggtagatcgc
pKRB2053	cgagctcaggaggaattcacc
	ctctcatccgccaaaac
pKRB2100	cgagctcttgatcgcgctaaatactgcttcaccac
	cccaagctttcagttacggaaagggttatgaccgttac
pKRB2104	gttcgaaaacccgtggttgcgctggtacccagt
	actgggtaccagcgcaaccacgggttttcgaac
pKRB2107	ggtgcctgttgtcctggctgttgtgctggtacccagtatgacgatagca
	accagcacaacagccaggacaacaggcaccacgggttttcgaaccgcta
pKRB116	cgagctcgtgaaggaggctcgagccatgaaattcagccataaaattgttgctgcg
	aaaactgcagacactttgaatttattcaagattgcatcctgttcg
YKN12	gaatgaagatatcgagcacagccatactgtcgatcatcatttaagacccactttcacatt
	aaaaaggccgcttacgcggccttagtgattacacgttgtactaagcacttgtctcctg
	ggtggttcgccgccgctttag
	aaaaaggccgcttacgcggccttagtgattacacgttgtattacttgtacagctcgtccatgccc
MBRT02	gctggtgcgccgccgcttcccgctgaagccgcgcccggaattaagacccactttcacatt
	tgaaaaaggcgacacattggcatgtcgccttttttattgcctaagcacttgtctcctg
	tggctatttacttcgtgccgctgttc
	tgaaaaaggcgacacattggcatgtcgccttttttattgcttacttgtacagctcgtccatgcc

References

Adams MD, Goglin K, Molyneaux N, Hujer KM, Lavender H, Jamison JJ, MacDonald IJ, Martin KM, Russo T, Campagnari AA, Hujer AM, Bonomo RA, Gill SR (2008) Comparative genome sequence analysis of multidrug-resistant Acinetobacter baumannii. *J Bacteriol* **190:** 8053-8064

Aires JR, Nikaido H (2005) Aminoglycosides are captured from both periplasm and cytoplasm by the AcrD multidrug efflux transporter of *Escherichia coli*. *J Bacteriol* **187:** 1923-1929

Altmann SW, Davis HR, Jr., Zhu LJ, Yao X, Hoos LM, Tetzloff G, Iyer SP, Maguire M, Golovko A, Zeng M, Wang L, Murgolo N, Graziano MP (2004) Niemann-Pick C1 Like 1 protein is critical for intestinal cholesterol absorption. *Science* **303:** 1201-1204

Baba T, Ara T, Hasegawa M, Takai Y, Okumura Y, Baba M, Datsenko KA, Tomita M, Wanner BL, Mori H (2006) Construction of *Escherichia coli* K-12 in-frame, single-gene knockout mutants: the Keio collection. *Mol Syst Biol* **2:** 2006 0008

Bansal T, Alaniz RC, Wood TK, Jayaraman A (2010) The bacterial signal indole increases epithelial-cell tight-junction resistance and attenuates indicators of inflammation. *Proc Natl Acad Sci U S A* **107:** 228-233

Blankenhorn D, Phillips J, Slonczewski JL (1999) Acid- and base-induced proteins during aerobic and anaerobic growth of Escherichia coli revealed by two-dimensional gel electrophoresis. *J Bacteriol* **181:** 2209-2216

Bochner BR, Huang HC, Schieven GL, Ames BN (1980) Positive selection for loss of tetracycline resistance. *J Bacteriol* **143:** 926-933

Bueschkens DH, Stiles ME (1984) *Escherichia coli* variants for gas and indole production at elevated incubation temperatures. *Appl Environ Microbiol* **48:** 601-605

Bush K, Jacoby GA, Medeiros AA (1995) A functional classification scheme for

beta-lactamases and its correlation with molecular structure. *Antimicrob Agents Chemother* **39:** 1211-1233

Chant EL, Summers DK (2007) Indole signalling contributes to the stable maintenance of *Escherichia coli* multicopy plasmids. *Mol Microbiol* **63:** 35-43

Datsenko KA, Wanner BL (2000) One-step inactivation of chromosomal genes in *Escherichia coli* K-12 using PCR products. *Proc Natl Acad Sci U S A* **97:** 6640-6645

Davies J, Davies D (2010) Origins and evolution of antibiotic resistance. *Microbiol Mol Biol Rev* **74:** 417-433

Deininger KN, Horikawa A, Kitko RD, Tatsumi R, Rosner JL, Wachi M, Slonczewski JL (2011) A requirement of TolC and MDR efflux pumps for acid adaptation and GadAB induction in *Escherichia coli*. *PLoS One* **6:** e18960

Di Martino P, Merieau A, Phillips R, Orange N, Hulen C (2002) Isolation of an *Escherichia coil* strain mutant unable to form biofilm on polystyrene and to adhere to human pneumocyte cells: involvement of tryptophanase. *Can J Microbiol* **48:** 132-137

Du D, Wang Z, James NR, Voss JE, Klimont E, Ohene-Agyei T, Venter H, Chiu W, Luisi BF (2014) Structure of the AcrAB-TolC multidrug efflux pump. *Nature* **509:** 512-515

Dzidic S, Suskovic J, Kos B (2008) Antibiotic resistance mechanisms in bacteria: Biochemical and genetic aspects. *Food Technology and Biotechnology* **46:** 11-21

Garau G, Garcia-Saez I, Bebrone C, Anne C, Mercuri P, Galleni M, Frere JM, Dideberg O (2004) Update of the standard numbering scheme for class B β-lactamases. *Antimicrob Agents Chemother* **48:** 2347-2349

Gelband H, Laxminarayan R (2015) Tackling antimicrobial resistance at global and local scales. *Trends Microbiol* **23:** 524-526

Griffin BA, Adams SR, Tsien RY (1998) Specific covalent labeling of recombinant protein molecules inside live cells. *Science* **281:** 269-272

Guzman LM, Belin D, Carson MJ, Beckwith J (1995) Tight regulation, modulation, and

high-level expression by vectors containing the arabinose P_{BAD} promoter. *J Bacteriol* **177:** 4121-4130

Hirakawa H, Inazumi Y, Masaki T, Hirata T, Yamaguchi A (2005) Indole induces the expression of multidrug exporter genes in *Escherichia coli*. *Mol Microbiol* **55:** 1113-1126

Hirakawa H, Kodama T, Takumi-Kobayashi A, Honda T, Yamaguchi A (2009) Secreted indole serves as a signal for expression of type III secretion system translocators in enterohaemorrhagic *Escherichia coli* O157:H7. *Microbiology* **155:** 541-550

Hiremath G, Hyakutake A, Yamamoto K, Ebisawa T, Nakamura T, Nishiyama S, Homma M, Kawagishi I (2015) Hypoxia-induced localization of chemotaxis-related signaling proteins in *Vibrio cholerae*. *Mol Microbiol* **95:** 780-790

Hoffmann C, Gaietta G, Zurn A, Adams SR, Terrillon S, Ellisman MH, Tsien RY, Lohse MJ (2010) Fluorescent labeling of tetracysteine-tagged proteins in intact cells. *Nat Protoc* **5:** 1666-1677

Kawamura-Sato K, Shibayama K, Horii T, Iimuma Y, Arakawa Y, Ohta M (1999) Role of multiple efflux pumps in *Escherichia coli* in indole expulsion. *FEMS Microbiol Lett* **179:** 345-352

Kitagawa M, Ara T, Arifuzzaman M, Ioka-Nakamichi T, Inamoto E, Toyonaga H, Mori H (2005) Complete set of ORF clones of *Escherichia coli* ASKA library (a complete set of *E. coli* K-12 ORF archive): unique resources for biological research. *DNA Res* **12:** 291-299

Knarreborg A, Beck J, Jensen MT, Laue A, Agergaard N, Jensen BB (2002) Effect of non-starch polysaccharides on production and absorption of indolic compounds in entire male pigs. *Animal Science* **74:** 445-453

Kobayashi A, Hirakawa H, Hirata T, Nishino K, Yamaguchi A (2006) Growth phase-dependent expression of drug exporters in *Escherichia coli* and its contribution to drug tolerance. *J Bacteriol* **188:** 5693-5703

Kobayashi N, Tamura N, van Veen HW, Yamaguchi A, Murakami S (2014) β-Lactam

selectivity of multidrug transporters AcrB and AcrD resides in the proximal binding pocket. *J Biol Chem* **289:** 10680-10690

Kofoid EC, Parkinson JS (1988) Transmitter and receiver modules in bacterial signaling proteins. *Proc Natl Acad Sci U S A* **85:** 4981-4985

Koronakis V, Sharff A, Koronakis E, Luisi B, Hughes C (2000) Crystal structure of the bacterial membrane protein TolC central to multidrug efflux and protein export. *Nature* **405:** 914-919

Kusumi A, Sako Y, Yamamoto M (1993) Confined lateral diffusion of membrane receptors as studied by single particle tracking (nanovid microscopy). Effects of calcium-induced differentiation in cultured epithelial cells. *Biophys J* **65:** 2021-2040

Lambert PA (2002) Mechanisms of antibiotic resistance in *Pseudomonas aeruginosa*. *J R Soc Med* **95 Suppl 41:** 22-26

Leake MC, Chandler JH, Wadhams GH, Bai F, Berry RM, Armitage JP (2006) Stoichiometry and turnover in single, functioning membrane protein complexes. *Nature* **443:** 355-358

Lee J, Jayaraman A, Wood TK (2007) Indole is an inter-species biofilm signal mediated by SdiA. *BMC Microbiol* **7:** 42

Lee JH, Lee J (2010) Indole as an intercellular signal in microbial communities. *FEMS Microbiol Rev* **34:** 426-444

Leyden JJ (1985) Absorption of minocycline hydrochloride and tetracycline hydrochloride. Effect of food, milk, and iron. *J Am Acad Dermatol* **12:** 308-312

Li G, Young KD (2013) Indole production by the tryptophanase TnaA in *Escherichia coli* is determined by the amount of exogenous tryptophan. *Microbiology* **159:** 402-410

Li XZ, Nikaido H (2009) Efflux-mediated drug resistance in bacteria: an update. *Drugs* **69:** 1555-1623

Li Y, Cole K, Altman S (2003) The effect of a single, temperature-sensitive mutation on global gene expression in *Escherichia coli*. *RNA* **9:** 518-532

Ma D, Alberti M, Lynch C, Nikaido H, Hearst JE (1996) The local repressor AcrR plays a modulating role in the regulation of *acrAB* genes of *Escherichia coli* by global stress signals. *Mol Microbiol* **19:** 101-112

Ma D, Cook DN, Alberti M, Pon NG, Nikaido H, Hearst JE (1993) Molecular cloning and characterization of *acrA* and *acrE* genes of *Escherichia coli*. *J Bacteriol* **175:** 6299-6313

Ma D, Cook DN, Alberti M, Pon NG, Nikaido H, Hearst JE (1995) Genes *acrA* and *acrB* encode a stress-induced efflux system of *Escherichia coli*. *Mol Microbiol* **16:** 45-55

Matagne A, Dubus A, Galleni M, Frere JM (1999) The beta-lactamase cycle: a tale of selective pressure and bacterial ingenuity. *Nat Prod Rep* **16:** 1-19

McMurry L, Petrucci RE, Jr., Levy SB (1980) Active efflux of tetracycline encoded by four genetically different tetracycline resistance determinants in *Escherichia coli*. *Proc Natl Acad Sci U S A* **77:** 3974-3977

McRae SR, Brown CL, Bushell GR (2005) Rapid purification of EGFP, EYFP, and ECFP with high yield and purity. *Protein Expr Purif* **41:** 121-127

Melander RJ, Minvielle MJ, Melander C (2014) Controlling bacterial behavior with indole-containing natural products and derivatives. *Tetrahedron* **70:** 6363-6372

Morar M, Wright GD (2010) The genomic enzymology of antibiotic resistance. *Annu Rev Genet* **44:** 25-51

Murakami S, Nakashima R, Yamashita E, Matsumoto T, Yamaguchi A (2006) Crystal structures of a multidrug transporter reveal a functionally rotating mechanism. *Nature* **443:** 173-179

Murakami S, Nakashima R, Yamashita E, Yamaguchi A (2002) Crystal structure of bacterial multidrug efflux transporter AcrB. *Nature* **419:** 587-593

Murakami S, Yamaguchi A (2003) Multidrug-exporting secondary transporters. *Curr Opin Struct Biol* **13:** 443-452

Nguyen-Disteche M, Leyh-Bouille M, Ghuysen JM (1982) Isolation of the membrane-bound

26 000-Mr penicillin-binding protein of *Streptomyces* strain K15 in the form of a penicillin-sensitive D-alanyl-D-alanine-cleaving transpeptidase. *Biochem J* **207:** 109-115

Nikaido H (1998) Antibiotic resistance caused by gram-negative multidrug efflux pumps. *Clin Infect Dis* **27 Suppl 1:** S32-41

Nikaido H (2000) How do exported proteins and antibiotics bypass the periplasm in Gram-negative bacterial cells? *Trends Microbiol* **8:** 481-483

Nishino K, Honda T, Yamaguchi A (2005) Genome-wide analyses of *Escherichia coli* gene expression responsive to the BaeSR two-component regulatory system. *J Bacteriol* **187:** 1763-1772

Nishino K, Yamada J, Hirakawa H, Hirata T, Yamaguchi A (2003) Roles of TolC-dependent multidrug transporters of *Escherichia coli* in resistance to beta-lactams. *Antimicrob Agents Chemother* **47:** 3030-3033

Nishino K, Yamaguchi A (2001a) Analysis of a complete library of putative drug transporter genes in *Escherichia coli*. *J Bacteriol* **183:** 5803-5812

Nishino K, Yamaguchi A (2001b) Overexpression of the response regulator *evgA* of the two-component signal transduction system modulates multidrug resistance conferred by multidrug resistance transporters. *J Bacteriol* **183:** 1455-1458

Nishino K, Yamaguchi A (2002) EvgA of the two-component signal transduction system modulates production of the *yhiUV* multidrug transporter in *Escherichia coli*. *J Bacteriol* **184:** 2319-2323

Nishiyama S, Suzuki D, Itoh Y, Suzuki K, Tajima H, Hyakutake A, Homma M, Butler-Wu SM, Camilli A, Kawagishi I (2012) Mlp24 (McpX) of *Vibrio cholerae* implicated in pathogenicity functions as a chemoreceptor for multiple amino acids. *Infect Immun* **80:** 3170-3178

Nishiyama S, Takahashi Y, Yamamoto K, Suzuki D, Itoh Y, Sumita K, Uchida Y, Homma M, Imada K, Kawagishi I (2016) Identification of a *Vibrio cholerae* chemoreceptor that senses

taurine and amino acids as attractants. *Sci Rep* **6:** 20866

Oh D, Yu Y, Lee H, Wanner BL, Ritchie K (2014) Dynamics of the serine chemoreceptor in the *Escherichia coli* inner membrane: a high-speed single-molecule tracking study. *Biophys J* **106:** 145-153

Okusu H, Ma D, Nikaido H (1996) AcrAB efflux pump plays a major role in the antibiotic resistance phenotype of *Escherichia coli* multiple-antibiotic-resistance (Mar) mutants. *J Bacteriol* **178:** 306-308

Ormo M, Cubitt AB, Kallio K, Gross LA, Tsien RY, Remington SJ (1996) Crystal structure of the *Aequorea victoria* green fluorescent protein. *Science* **273:** 1392-1395

Paulsen IT, Brown MH, Skurray RA (1996) Proton-dependent multidrug efflux systems. *Microbiol Rev* **60:** 575-608

Pedelacq JD, Cabantous S, Tran T, Terwilliger TC, Waldo GS (2006) Engineering and characterization of a superfolder green fluorescent protein. *Nat Biotechnol* **24:** 79-88

Perez A, Poza M, Aranda J, Latasa C, Medrano FJ, Tomas M, Romero A, Lasa I, Bou G (2012) Effect of transcriptional activators SoxS, RobA, and RamA on expression of multidrug efflux pump AcrAB-TolC in *Enterobacter cloacae*. *Antimicrob Agents Chemother* **56:** 6256-6266

Pinero-Fernandez S, Chimerel C, Keyser UF, Summers DK (2011) Indole transport across *Escherichia coli* membranes. *J Bacteriol* **193:** 1793-1798

Putman M, van Veen HW, Konings WN (2000) Molecular properties of bacterial multidrug transporters. *Microbiol Mol Biol Rev* **64:** 672-693

Raffa RG, Raivio TL (2002) A third envelope stress signal transduction pathway in *Escherichia coli*. *Mol Microbiol* **45:** 1599-1611

Rosenberg EY, Ma D, Nikaido H (2000) AcrD of *Escherichia coli* is an aminoglycoside efflux pump. *J Bacteriol* **182:** 1754-1756

Sako Y, Minoghchi S, Yanagida T (2000) Single-molecule imaging of EGFR signalling on the

surface of living cells. *Nat Cell Biol* **2:** 168-172

Shallcross LJ, Howard SJ, Fowler T, Davies SC (2015) Tackling the threat of antimicrobial resistance: from policy to sustainable action. *Philos Trans R Soc Lond B Biol Sci* **370:** 20140082

Shimomura O, Johnson FH, Saiga Y (1962) Extraction, purification and properties of aequorin, a bioluminescent protein from the luminous hydromedusan, Aequorea. *J Cell Comp Physiol* **59:** 223-239

Smith DA (1998) A quantitative method for the detection of edges in noisy time-series. *Philos Trans R Soc Lond B Biol Sci* **353:** 1969-1981

Smith T (1897) A Modification of the Method for Determining the Production of Indol by Bacteria. *J Exp Med* **2:** 543-547

Spratt BG (1977) Properties of the penicillin-binding proteins of *Escherichia coli* K12. *Eur J Biochem* **72:** 341-352

Stewart V, Yanofsky C (1985) Evidence for transcription antitermination control of tryptophanase operon expression in *Escherichia coli* K-12. *J Bacteriol* **164:** 731-740

Stover CK, Pham XQ, Erwin AL, Mizoguchi SD, Warrener P, Hickey MJ, Brinkman FS, Hufnagle WO, Kowalik DJ, Lagrou M, Garber RL, Goltry L, Tolentino E, Westbrock-Wadman S, Yuan Y, Brody LL, Coulter SN, Folger KR, Kas A, Larbig K, Lim R, Smith K, Spencer D, Wong GK, Wu Z, Paulsen IT, Reizer J, Saier MH, Hancock RE, Lory S, Olson MV (2000) Complete genome sequence of *Pseudomonas aeruginosa* PAO1, an opportunistic pathogen. *Nature* **406:** 959-964

Strateva T, Yordanov D (2009) *Pseudomonas aeruginosa* - a phenomenon of bacterial resistance. *J Med Microbiol* **58:** 1133-1148

Sulavik MC, Houseweart C, Cramer C, Jiwani N, Murgolo N, Greene J, DiDomenico B, Shaw KJ, Miller GH, Hare R, Shimer G (2001) Antibiotic susceptibility profiles of *Escherichia coli* strains lacking multidrug efflux pump genes. *Antimicrob Agents*

Chemother **45:** 1126-1136

Swulius MT, Jensen GJ (2012) The helical MreB cytoskeleton in *Escherichia coli* MC1000/pLE7 is an artifact of the N-Terminal yellow fluorescent protein tag. *J Bacteriol* **194:** 6382-6386

Tamura N, Murakami S, Oyama Y, Ishiguro M, Yamaguchi A (2005) Direct interaction of multidrug efflux transporter AcrB and outer membrane channel TolC detected via site-directed disulfide cross-linking. *Biochemistry* **44:** 11115-11121

Tikhonova EB, Zgurskaya HI (2004) AcrA, AcrB, and TolC of *Escherichia coli* form a stable intermembrane multidrug efflux complex. *J Biol Chem* **279:** 32116-32124

Tokunaga M, Kitamura K, Saito K, Iwane AH, Yanagida T (1997) Single molecule imaging of fluorophores and enzymatic reactions achieved by objective-type total internal reflection fluorescence microscopy. *Biochem Biophys Res Commun* **235:** 47-53

Tso WW, Adler J (1974) Negative chemotaxis in *Escherichia coli*. *J Bacteriol* **118:** 560-576

Vega NM, Allison KR, Khalil AS, Collins JJ (2012) Signaling-mediated bacterial persister formation. *Nat Chem Biol* **8:** 431-433

Walsh TR, Toleman MA, Poirel L, Nordmann P (2005) Metallo-beta-lactamases: the quiet before the storm? *Clin Microbiol Rev* **18:** 306-325

Watanabe R, Doukyu N (2012) Contributions of mutations in *acrR* and *marR* genes to organic solvent tolerance in *Escherichia coli*. *AMB Express* **2:** 58

Webber MA, Piddock LJ (2003) The importance of efflux pumps in bacterial antibiotic resistance. *J Antimicrob Chemother* **51:** 9-11

West AH, Stock AM (2001) Histidine kinases and response regulator proteins in two-component signaling systems. *Trends Biochem Sci* **26:** 369-376

Wyeth FJ (1919) The effects of acids, alkalies, and sugars on the growth and indole formation of *Bacillus coli*: A Report to the Medical Research Committee. *Biochem J* **13:** 10-24

Yamamoto K, Tamai R, Yamazaki M, Inaba T, Sowa Y, Kawagishi I (2016)

Substrate-dependent dynamics of the multidrug efflux transporter AcrB of *Escherichia coli*. *Sci Rep* **6:** 21909

Yao XQ, Kenzaki H, Murakami S, Takada S (2010) Drug export and allosteric coupling in a multidrug transporter revealed by molecular simulations. *Nat Commun* **1:** 117

Zgurskaya HI, Nikaido H (1999) Bypassing the periplasm: reconstitution of the AcrAB multidrug efflux pump of *Escherichia coli*. *Proc Natl Acad Sci U S A* **96:** 7190-7195

Notes

The results presented in Chapter II of this dissertation were published as the following paper:

Yamamoto, K., Tamai, R., Yamazaki, M., Inaba, T., Sowa, Y., and Kawagishi, I. (2016) Substrate-dependent dynamics of the multidrug efflux transporter AcrB of *Escherichia coli*. *Sci. Rep.* **6:** 21909.

The results presented in Chapter IV of this dissertation were published as the following papers:

Hiremath, G., Hyakutake, A., Yamamoto, K., Ebisawa, T., Nakamura, T., Nishiyama, S., Homma, M., and Kawagishi, I. (2015) Hypoxia-induced localization of chemotaxis-related signaling proteins in *Vibrio cholerae*. *Mol. Microbiol.* **95:** 780-790.

Nishiyama, S.¶, Takahashi Y.¶, Yamamoto, K.¶, Suzuki, D., Itoh, Y., Sumita, K., Uchida, Y., Homma, M., Imada, K., and Kawagishi, I. (2016) Identification of a *Vibrio cholerae* chemoreceptor that senses taurine and amino acids as attractants. *Sci. Rep.* **6:** 20866.

¶These authors contributed equally to this work.